Updated assessment of rock avalanche hazard and risk at Plateau Hut, Aoraki / Mount Cook National Park

SC Cox

GNS Science Consultancy Report 2021/83
November 2021

GNS SCIENCE
TE PŪ AO

DISCLAIMER

This report has been prepared by the Institute of Geological and Nuclear Sciences Limited (GNS Science) exclusively for and under contract to the Department of Conservation – Te Papa Atawhai. Unless otherwise agreed in writing by GNS Science, GNS Science accepts no responsibility for any use of or reliance on any contents of this report by any person other than the Department of Conservation and shall not be liable to any person other than the Department of Conservation, on any ground, for any loss, damage or expense arising from such use or reliance.

Use of Data:

Date that GNS Science can use associated data: November 2021

BIBLIOGRAPHIC REFERENCE

Cox SC. 2021. Updated assessment of rock avalanche hazard and risk at Plateau Hut, Aoraki / Mount Cook National Park. Lower Hutt (NZ): GNS Science. 37 p. Consultancy Report 2021/83.

CONTENTS

FIGURES

TABLES

EXECUTIVE SUMMARY

The hazard and risk from rock and ice avalanches at Plateau Hut in the Aoraki / Mount Cook National Park (AMCNP) has been re-analysed in this report. It updates calculations by Hancox and Thomson (2013b) using latest science on the frequency and occurrence of local landslides, new work on the probability of an Alpine Fault earthquake and recent studies on earthquake-induced landslides elsewhere in New Zealand. It also follows methodology in the standardised guidelines for natural hazard risk analysis on public conservation lands and waters (de Vilder and Massey 2020a, 2020b). Plateau Hut is classed as a 'Backcountry Adventure' site within the Department of Conservation (DOC)'s visitor categories, which is used mostly but not exclusively by Remote Seeker risk-taker visitors (climbers), who have a high risk tolerance because of the activity they are engaging in.

One quantification of risk uses a metric of the individual risk per day per trip to visitors. It provides a daily probability of death by rock and ice avalanches for a theoretical imaginary person present at the hut for 14 hours per day at ΣP_{IRPD} = 1.0 to 1.5 x 10^{-5}. The 14 hr/day is an average occupancy of visitors derived by DOC from their visitor statistics and experience. The risk is composite from both non-earthquake (~28–32% of total risk) and earthquake-induced (~13–27% of the total) landslides, which are quantified with a relatively high degree of confidence, and the possibility of a large ice avalanche induced by an earthquake (potentially ~41–58% of the total risk). There is little information available to assess and quantify triggering of ice-cliff collapse during earthquakes, or large ice avalanche runout, so there is lower confidence in this component of risk. The possibility that ice cliffs will not always collapse during an Alpine Fault earthquake, or an ice avalanche will not always reach the hut, means that the ice avalanche risk value presented is likely a maximum and therefore conservative. Further work to understand ice avalanches can be expected to decrease total risk values at the hut.

Other metrics provided include the local personal risk (LPR) at ΣP_{LPR} = 6.3 to 9.0 x 10^{-3}. LPR is the annual probability of death for a theoretical imaginary person present at the hut for 100% of the time – 24 hours per day, 365 days per year. Measures of 'societal' risk of multiple fatalities from a rock or ice avalanche impacting Plateau Hut have been calculated on the basis of 2019 occupancy statistics, before visitor numbers were affected by COVID-19. The annual risk of death of ≥5 people is $\Sigma P_{SOC\ (N\geq5)}$ = 9.6 x 10^{-4} to 1.4 x 10^{-3}, whereas ≥30 people is $\Sigma P_{SOC\ (N\geq30)}$ = 1.8 to 2.7 x 10^{-4}.

Individual risk per day of staying at the hut (ΣP_{IRPD}) is significantly lower than during a climb of Aoraki / Mount Cook, about the same as during a helicopter flying to and from the hut, and is comparable with a number of other adventure activities popular in New Zealand. Societal risks (ΣP_{SOC}) are lower than those from past New Zealand earthquakes, or storm and flood events, that have killed multiple people. These estimates of risk can be evaluated against DOC's present visitor management strategy and whether they are tolerable or intolerable and if risk reduction is needed. This is expected to vary in accordance with the risk tolerance profile of climbers and other sporadic users or more regular visits by mountain guides and staff.

This page left intentionally blank.

1.0 BACKGROUND

This report has been prepared by the Institute of Geological and Nuclear Sciences Limited (GNS Science) for the Department of Conservation (DOC), in response to a request from Don Bogie (Principal Advisor Visitor Risk) to review the rock avalanche hazard and risk at Plateau Hut in the Aoraki / Mount Cook National Park (AMCNP; Figure 1.1). Plateau Hut is classed as a 'Backcountry Adventure' site within DOC's visitor categories, which is used mostly but not exclusively by Remote Seeker risk-taker visitors (climbers), who have a high risk tolerance because of the activity they are engaging in.

A hazard assessment was previously carried out in 2013 following a large rock avalanche from Mt Haast that crossed Grand Plateau and passed nearby the hut (Hancox and Thomson 2013a, 2013b). Since that time, warm summers and/or heavy wet snowfall events have continued to trigger a number of moderate (10^3–10^4 m^3) to large (≥10^5 m^3) -sized landslides throughout the central Southern Alps, while other rock avalanches, such as the Hillary Ridge of Aoraki (14 July 2014), have been seemingly spontaneous. Significant-sized rock avalanches from Vancouver and Silberhorn in summer 2020 were followed by a second larger collapse from Silberhorn onto Grand Plateau in December 2020. Shortly after, there were collapses from Mount Darwin (Tasman Glacier) and Mount Hutton (Liebig Range) in January–February 2021. Collectively, the events raised awareness of local rockfall and rock avalanche hazard. Given the number of recent events, DOC want to check whether the Plateau Hut hazard analysis remains valid and its facility management still appropriate.

This report aims to provide an 'Advanced-level specific point site analysis' based on methodology of de Vilder and Massey (2020a, 2020b), following AGS (2007) and JTC-1 (Fell et al. 2008) guidelines and standards. To analyse the hazard and estimate risk at Plateau Hut, the report draws on the latest observations of landslides and unpublished data being collated as part of the 'Matariki Project'.[1] This Ministry of Business, Innovation and Employment (MBIE)-funded Smart Ideas project, awarded to the University of Otago and GNS Science, has employed photogrammetry from satellite and aerial imagery to generate digital surface models at metre-scale resolution to quantify landscape changes. These enabled an up-to-date inventory of landslide events to be collated throughout the AMCNP.

1.1 Hazard at Plateau Hut

Plateau Hut is situated at 2200 m on a broad ridge of greywacke bedrock about 4.5 km northeast of Aoraki / Mount Cook on the eastern side of Grand Plateau (Figure 1.1). The hut is on an elevated site, sitting above the plateau and Hochstetter Glacier icefall, some distance from steep slopes. An original hut was constructed in 1963/64 but was replaced at the same location by a slightly larger hut in 2005. The new 33-bed hut tends to be most occupied during September–January. The 2017–2019 (pre-COVID-19) average for total bed nights per year was 1167, with an 'average visitor' spending 2.5 nights per visit (DOC, unpublished data).

No rock falls or rock and/or ice avalanches have affected the hut site since original construction in the early 1960s. However, the threat was well exemplified by the 11.8 Mm^3 collapse from Aoraki / Mount Cook on 13 December 1991 (Hancox et al. 1991; McSaveney 2002), which involved open-slope collapse of rock and overlying ice that passed within 400 m of the hut as debris surged down the Hochstetter icefall to Tasman Glacier (Figure 1.2A). A rock avalanche on 21 January 2013 from Mt Haast (0.8 Mm^3) came even closer, to within 250 m

1 See https://www.otago.ac.nz/surveying/potree/pub/mrc/projects/matariki

of the hut (Figure 1.2B; https://www.youtube.com/watch?v=E28_3uj9K0g; Hancox and Thomson 2013a). During summer 2020, there were two prominent rock avalanches from Silberhorn (between 23 and 28 January 2020) and Vancouver (between 11 February and 12 March 2020) (Figure 1.2C). A larger avalanche (0.16 Mm^3) from the same source area of Silberhorn on 31 December 2020 then came within 600 m of the hut when its flow turned southwards on Grand Plateau and started heading down the Hochstetter Glacier (Figure 1.2D).

The 2013 hazard assessment (Hancox and Thomson 2013b) rationalised that Plateau Hut is highly unlikely to be impacted by local geological hazards (foundation instability and collapse, or local rock fall). However, it indicated some possibility of hazard from very large rock or ice avalanches from steep slopes 3–4 km northwest to southwest of the site, particularly during strong shaking caused by an Alpine Fault earthquake.

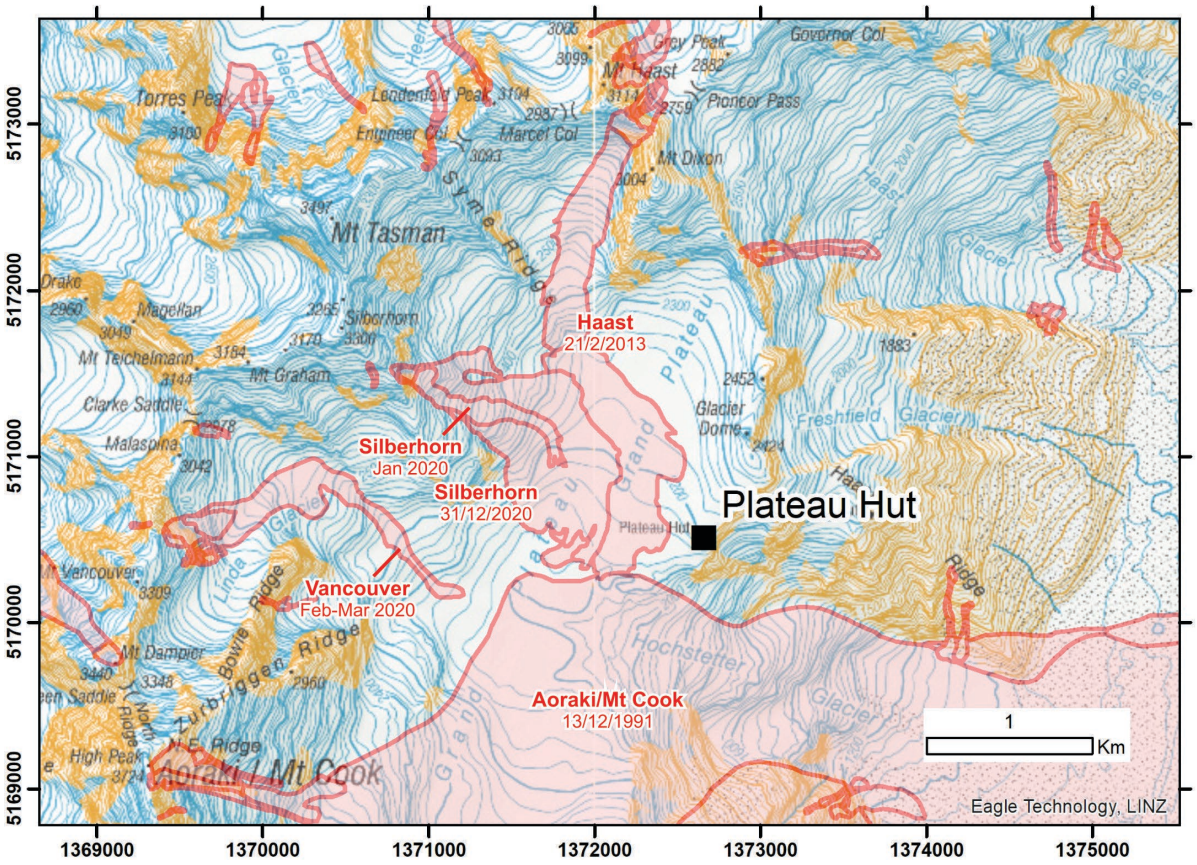

Figure 1.1 Overview map showing the setting of Plateau Hut, Grand Plateau and southeast-facing slopes from Silberhorn to Mt Dixon that present a rock avalanche hazard to the hut. Mapped outlines of past landslides are shown in red/pink, including the large rock avalanches from Aoraki / Mount Cook 1991, Haast 2013, Silberhorn and Vancouver 2020.

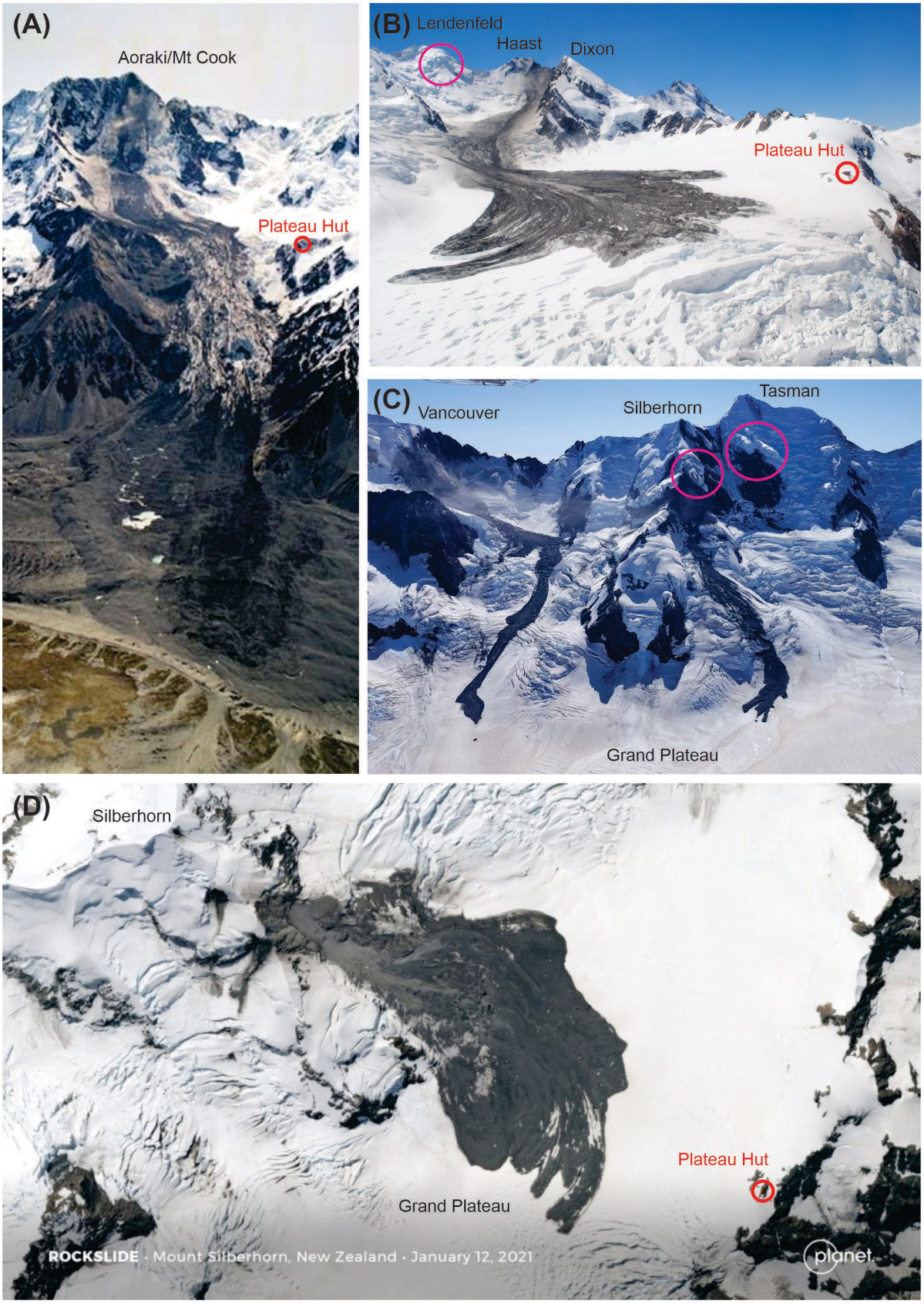

Figure 1.2 Examples of rock avalanches near Plateau Hut. (A) 1991 Aoraki / Mount Cook (Photo: L Homer, CN21418/12). (B) 2013 Mt Haast (Photo: R Thomson). (C) Vancouver and Silberhorn during January–March 2020 (Photo: G Macca, NIWA, 2020 Snowline Survey). Some notable ice cliffs of potential concern, present at the time the photograph was taken, have been annotated with larger pink circles. (D) Silberhorn in December 2020 (Planet Labs SkySat image on 12 January 2021).

1.2 New Information and Report Context

Since the 2013 hazard assessment was completed, there have been some significant changes in information available for quantifying hazards:

1. Through the Matariki Project, GNS Science has collated a large dataset on the frequency, magnitude and runout of recent rock avalanche events in AMCNP, where previously there were just a few known large events from throughout the Southern Alps to draw statistics from.
2. Recent work has greatly improved the knowledge of past Alpine Fault earthquakes, including the 75% probability of an earthquake in the next 50 years (Howarth et al. 2021) and the importance of rupture direction and length for the different style of earthquakes, aftershocks and ground motion simulations (Bradley et al. 2017).
3. There were widespread landslides induced during the 2016 Kaikōura earthquake, from which relationships between occurrence, ground shaking, slope angle, etc. (Massey et al. 2018, 2020) in greywacke bedrock provide a useful proxy for effects of shaking in the central Southern Alps. Models of earthquake-induced landslides are much improved.

However, there remains a substantial information gap around the possibility of earthquake-induced ice avalanches and their runout behaviour. There are no local New Zealand inventories, for example, from which this hazard can be fully quantified.

The aim of this report is to re-evaluate the total risk from both non-earthquake and earthquake-induced landslides in light of the above information and recent landslides near Plateau Hut. Although risk from earthquake-induced ice-cliff collapse and ice avalanches contains significant knowledge gaps, it can also be re-assessed in the context of the new information listed above.

1.3 Risk Analysis Method

This report follows guidelines of de Vilder and Massey (2020a, 2020b) to provide risk metrics that are now becoming standardised for adoption and use by DOC. The reader is referred to these more extensive reports for rationale behind methods, metrics and equations, as well as associated references to international literature justifying the adopted approach.

Local personal risk (LPR) is the annual probability of death by landslide for a theoretical imaginary person present at the hut 100% of the time (24 hours each day), which can be calculated as:

$$P_{LPR} = P_H \, x \, P_{S:H} \, x \, P_{T:S} \, x \, V \qquad \text{Equation 1.1}$$

where:

- P_H is the annual probability of a hazardous rock or ice avalanche event occurring.
- $P_{S:H}$ is the spatial probability of impact on the hut by a rock or ice avalanche.
- $P_{T:S}$ is the temporal spatial probability of a person being present in the hut. For LPR, this is set at 100% (24 hours per day).
- V is the vulnerability or probability of loss of life if the landslide impacts the hut.

Another metric proposed to be suitable for DOC (de Vilder and Massey 2020a) is the individual risk per day per trip for visitors. In this case:

$$P_{IRPD} = P_H \times P_{S:H} \times P_{T:S} \times V_{D:T}$$

$$= P_{LPR} \times (E/24) / 365.25 \quad \text{Equation 1.2}$$

where:

- $P_{T:S}$ is the temporal spatial probability, being the proportion of a day that a visitor is exposed to the hazard.
- E is average number of hours each day that a visitor is exposed to the hazard.
- *24* is the number of hours in each day.
- *365.25* is the number of days per year on average, accounting for leap years.

LPR is composite of metrics from all of the different types of landslides or landslides of different sizes. If the hazards are independent of each other, they can be summed; for example:

$$\Sigma P_{LPR} = P_{LPR(nonEQ)} + P_{LPR\ (EIL)} + P_{LPR\ (nonEII)} \quad \text{Equation 1.3}$$

where

- $P_{LPR(nonEQL)}$ is the annual LPR probability of a non-earthquake-related landslide.
- $P_{LPR(EIL)}$ is the annual LPR probability of an earthquake-induced landslide.
- $P_{LPR(nonEII)}$ is the annual LPR probability of a non-earthquake icefall.

Where the hazards result from the same causative event, such as a single earthquake, it has been recommended that probabilities should be estimated using the theory of unimodal bounds following de Morgan's rule (de Vilder and Massey 2020a). As an example, the upper and lower bound conditional probabilities are:

$$P_{(UB)} = 1 - (1-P_{(EIL)})(1-P_{(EII)}) \quad \text{Equation 1.4}$$

$$P_{(LB)} = max\ of\ P_{(EIL)}\ or\ P_{(EII)} \quad \text{Equation 1.5}$$

where

- $P_{(UB)}$ is the upper bound conditional probability of an earthquake-induced landslide or icefall.
- $P_{(LB)}$ is the lower bound conditional probability of an earthquake-induced landslide or icefall.
- $P_{(EIL)}$ is the annual probability of an earthquake-induced landslide.
- $P_{(EII)}$ is the annual probability of an earthquake-induced icefall.

A simplified 'societal' or 'group' risk can be calculated from a combination of the frequency of occurrence of a specified hazard and the likelihood that a specified number of people may be present and harmed in a single event. In this instance, an annual probability is calculated:

$$P_{SOC} = P_{LPR} \times P_{T:S(\geq N)} \quad \text{Equation 1.6}$$

where $P_{T:S(\geq N)}$ is the probability of ≥N people being present, based on the proportion of a year (number of days / 365.25 and hours per day) when there are ≥N visitors at the hut.

For this report, the probabilities listed above have either been derived directly from observations of landslides and assessment of features in AMCNP or rationalised from other landslide studies or comparative examples. Details of the source of data are provided in Sections 2 and 3.

2.0 LANDSLIDE HAZARD

2.1 Source Slopes and Pre-Disposing Factors

There seems credible potential for large avalanches of rock, rock and ice, or potentially even just ice (see below), from the slopes above Grand Plateau impacting on Plateau Hut (Figures 1.1 and 1.2). The slopes of particular threat are those from Silberhorn–Mt Tasman–Lendenfeld–Mt Haast–Mt Dixon. These face southeast, mostly with slope angles of between 20° and 60° but locally reaching as much as 80–85° over short distances of rock or ice cliffs. Snow and ice are widespread, covering bedrock composed of fractured and weakly cleaved greywacke (interlayered sandstone and argillite). Bedding layers have been aligned (transposed) within the rock mass into a sequence that dips uniformly (near-homoclinal) northwest into the slopes at between 45° and 55° (Cox and Barrell 2007). Given this underlying geology, and experience of rockfall and rock avalanches both here and nearby (e.g. Allen et al. 2011; Hancox and Thomson 2013a; McSaveney 2002), gravitational failure of the bedrock is expected to either involve rotation and toppling of bedding (typically failures of smaller volume) or involve wedge failures on secondary through-going fractures and joints developed at a high angle to bedding (mode for larger failures). There is no information available on any pre-disposing factors for ice-cliff collapse, other than observations that the scale of ice cliffs do change substantially over time (e.g. Figure 1.2; see also Hancox and Thomson 2013b).

To predict the possibility of failure from the slopes above Grand Plateau, a wider inventory of landslides is required from which there are sufficient numbers of landslides that statistically robust magnitude-frequency and source information can be defined, then used to derive an annual probability of a hazardous rock or ice avalanche event (P_H) occurring from the source slopes above the hut. A study area was selected to provide a proxy for those slopes above Plateau Hut, and collation of pre-disposing factors can inform where landslides are more likely to occur on such slopes. The study area, including three separate regions in the AMCNP, was selected where slopes have equivalent geology (underlain by moderate steeply northwest-dipping greywacke), slope (southeast-aspect, ≥30°), location and precipitation (beneath the Main Divide or the parallel Malte Brun Range), snow and ice cover (glaciated, >800 m elevation) and expected failure mode (scarp slopes at a high angle to bedding). The study area covers 219 km^2 from Barron Saddle (Mueller Glacier) to Harper Saddle (Hooker Glacier), Ball Pass (Mount Cook Range) to Mt Walter (Tasman Glacier), and Novara Peak (Murchison Glacier) to Sealy Pass (Godley Glacier). The study area and inventory of rock avalanches and large rockfalls within it, located as points coloured by size, are shown in Figure 2.1.

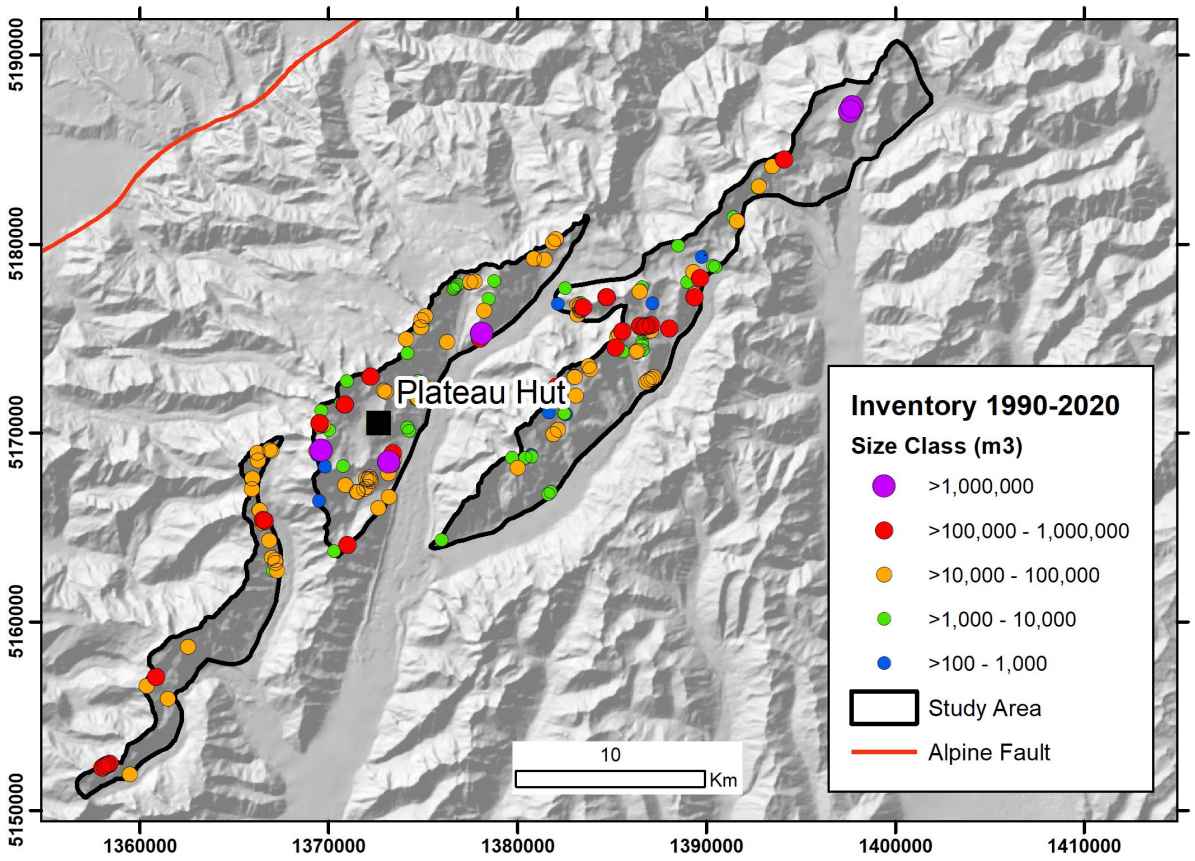

Figure 2.1 Map of the 219 km^2 landslide study area and inventory of 192 rock avalanches and large rockfalls that occurred between 1990 and 2020. Displayed on an 8 m shaded elevation model. The surface trace of the Alpine Fault (red line) is 18 km to the northwest, but, since the fault plane slopes beneath the mountains (dipping ~45–55° to the southeast), it sits closer to Plateau Hut at depth.

2.2 Inventory of Non-Earthquake Landslides

Rock avalanche and large rockfall events occur 'naturally', or semi-spontaneously without earthquake trigger, in the study area. There were 192 rock avalanches or large rockfalls in the study area between 1990 and 2020 that have been mapped manually in an unpublished GIS database (Figure 2.1, Cox and Sirguey, work in preparation[2]). The process used change detection and high-resolution imagery to improve earlier mapping (Cox and Barrell 2007; Allen et al. 2011) by mapping each event with separate source, path and deposit area polygon(s), then deriving a range of other attributes such as size, slope, aspect and elevation. Collapses during the 30-year period cover 1.44 km^2, equating to 0.02% of the study area per year.

The high-resolution digital surface models generated for the Matariki Project enable vertical changes of <1 m to be detected, but, with this degree of precision, seasonal variations in snow are also present in the change, so the timing of imagery can be important. Landslide volumes have been estimated by either (i) automated differencing of digital surface models generated from imagery (epochs 2017, 2013 and 2008), with manual corrections to account for local snow cover or (ii) estimates from topographic map dimensions (for landslides older than 2008) (Cox and Sirguey, in prep.). Uncertainties were quantified from the standard errors of the digital surface models, but these do not include effects of snow variation or digitising precision. Volume uncertainties are estimated to be between 4 and 10% in the Aoraki dataset, with smaller landslides having greater plan-view area uncertainty due to digitising

2 For further information on the Matariki Project, see www.otago.ac.nz/surveying/potree/pub/mrc/projects/matariki

precision and proportional volume of snow cover, whereas larger landslides have uncertainty dominated by the thickness estimation and simplifications into 3D. Importantly, the best-fit volume to area relationship for this inventory is Volume = 0.40*(Area)$^{1.35}$ (R^2 = 0.81), which shows consistency with scaling relationships determined for non-weathered greywacke debris avalanches and rockslides triggered during the Inangahua and Kaikōura earthquakes (Massey et al. 2020; de Vilder and Massey 2020b), which have scaling exponents of 1.1–1.4.

Slope angles in the study area and landslide polygons were calculated from an 8 m Digital Elevation Model (DEM; LINZ Data Service 2012, Figure 2.1).[3] Mean slope angles were derived for the landslide source areas and show that susceptibility to failure begins from about ≥30° (Figure 2.2A). When normalised against the proportion of all slopes within 5° bins from 0° to 90°, the normalised frequency (measured as number of events/km^2/year at different slope intervals) provides a proxy for the failure susceptibility in the study area. Albeit with a small deviation in the 70–75° category, the normalised frequency increases sensibly with steepening slope (Figure 2.2B).

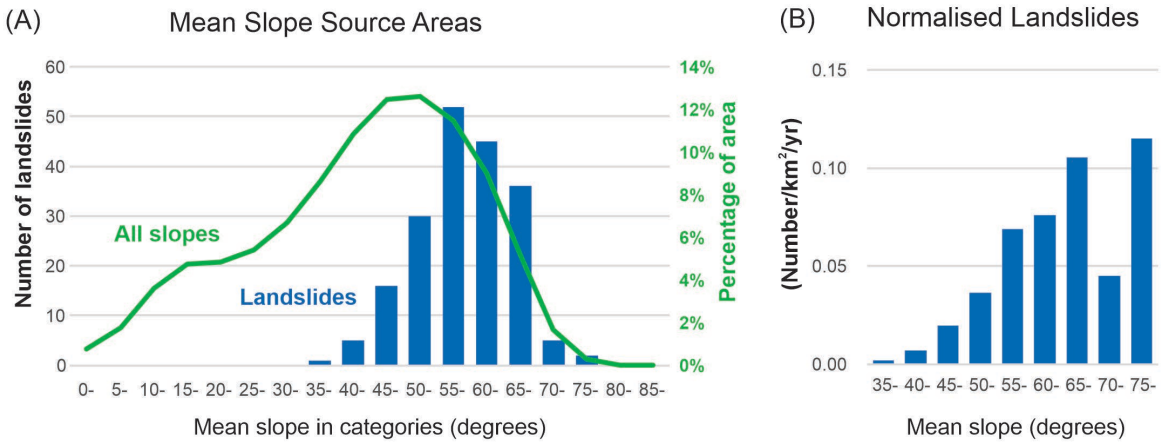

Figure 2.2 Histograms of mean topographic slope of landslide source areas in 5° bins. (A) All landslide source areas in the study area (blue) compared with percentage of all slopes (green line). (B) Source areas normalised by the proportion of slopes in the study area over 30 years of the inventory (in units of number/km^2/year).

2.3 Magnitude and Frequency of Non-Earthquake Landslides

There are 173 km^2 of slopes with potential to collapse (i.e. ≥ 30°) within the 219 km^2 study area. The landslide inventory, representing events in the 1990–2020 period, was subdivided by landslide volume into a series of order of magnitude categories. A magnitude-frequency model was generated for the 2.6 km^2 source area threatening Plateau Hut, based on the average number of landslides per year in each category times the fraction of the 2.6 km^2 source area compared with susceptible slopes in study area (173 km^2). Normalised over the 30-year period, values in N/yr were plotted as points at the geometric mean of each logarithmic volume bin (Figure 2.3, following de Vilder and Massey 2020b), which tends toward a linear log-log relationship for events ≥10,000 m^3. The linear best-fit equation to these points is N/yr = 59.3*Volume$^{-0.68}$ with R^2 = 0.99. The graph also shows a characteristic roll-over, suggesting either that the inventory is incomplete (under-sampled) for events <10,000 m^3 (cf. Stark and Hovius 2001; Malamud et al. 2004) or that there are different mechanisms

3 Although higher-resolution surface models do exist, they are epoch-dependent and contain temporal effects, such as variations in snow thickness, that are effectively 'smoothed' within the 8 m LINZ DEM. This DEM is also used as an input into the Earthquake-Induced Landslide (EIL) forecasting tool (Massey et al. 2021) used later in this report.

or processes influencing smaller event frequency. Ice field protection, for example, might be limiting exposure of the bedrock and local topographic variability, supressing the opportunity for smaller-scale failures. It is shown later that the smaller-volume events are unlikely to have runout sufficient to reach the hut (Sections 2.6 and 2.7), so the under-representation of smaller events is unlikely to be problematic. The magnitude-frequency distribution is the key basis on which the annual probability of non-earthquake landslides ($P_{H(nonEQL)}$) at different size categories has been estimated for the source slopes above Grand Plateau (see Section 4.1).

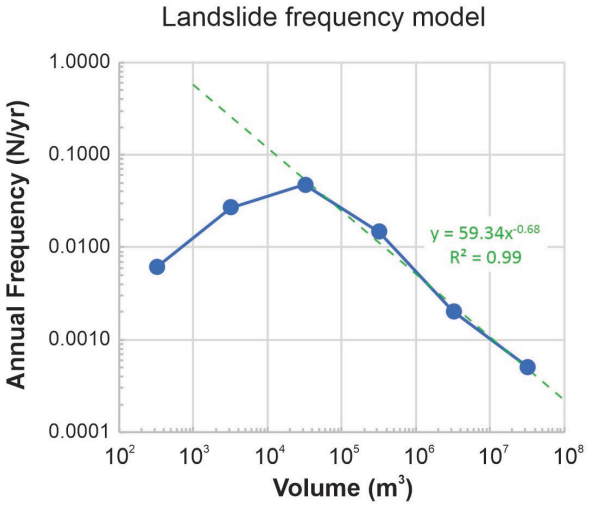

Figure 2.3 Landslide frequency magnitude distribution curve for the 2.6 km^2 source area. A linear trendline (green) can be fitted for volume categories >10,000 m^3. Points representing volume class ranges are plotted at the geometric mean of each category (following de Vilder and Massey 2020b).

2.4 Earthquake-Induced Landslides

There is widespread recognition of the possibility of landslides in the Southern Alps induced by an Alpine Fault earthquake (e.g. Orchiston et al. 2018). Recent work by Howarth et al. (2021) indicated that there is a 75% probability of an earthquake on the central Alpine Fault in the next 50 years, and two different modes (styles) of earthquakes, but was unable to define whether the next earthquake is expected to be a M_W 7–8 or M_W ≥8. The large size and frequent recurrence of earthquakes on the Alpine Fault means that it dominates the local seismic shaking and hazard probability (Stirling et al. 2012). For the purpose of this study, and as shown by Hancox and Thomson (2013b), other potential seismic sources (see Cox et al. 2012) are considered negligible when compared with imminent hazard from the Alpine Fault.

There are a variety of possible rupture directions, mode switching and rupture lengths, stress drops, shaking distributions and topographic amplification associated with an Alpine Fault event. Regardless of these variations, there is some consensus that the central Southern Alps will experience very strong to severe shaking at modified Mercalli intensities (MMI) of at least MMI 7–9 during an Alpine Fault earthquake (Bradley et al. 2017; Orchiston et al. 2018). One way to estimate local ground motion and its dependence on location of an earthquake, rupture length, attenuation with distance and class of ground is using ShakeMapNZ (Horspool et al. 2015), which provides local prediction of peak ground acceleration (PGA). Although it does not account for effects of rupture directivity or local topographic amplification, modelling of a M_W 8.2 earthquake (epicentre at 167.816°E -44.533°, southern end, depth 6 km) rupture of the fault predicts PGA = 0.36 g for subsoil Class B (rock) in the landslide source area above Plateau Hut and a 0.25–0.40 g range for the wider study area (Figure 2.4, from unpublished work of T Goded, GNS Science).

The levels of local shaking from an Alpine Fault earthquake, whether it is a M_W 7–8 or M_W ≥8, can be expected to provide high to very high opportunity for triggering landslides from susceptible slopes in the central Southern Alps (Hancox et al. 2002). The associated aftershock sequence (van Houtte and Gerstenberger 2019) is also likely to exceed MMI = 5 and PGA ≥0.2 g thresholds of ground shaking needed to induce or re-activate landslides (Hancox et al. 2002; Massey et al. 2018). Any greywacke bedrock slope with an angle of ≥30° in the central Southern Alps can be assumed capable of generating landslides during an earthquake, but only a proportion of these slopes will actually fail. The local probability of failure ($P_{H(EIL)}$) must therefore be some proportion of the probability of the earthquake shaking itself.

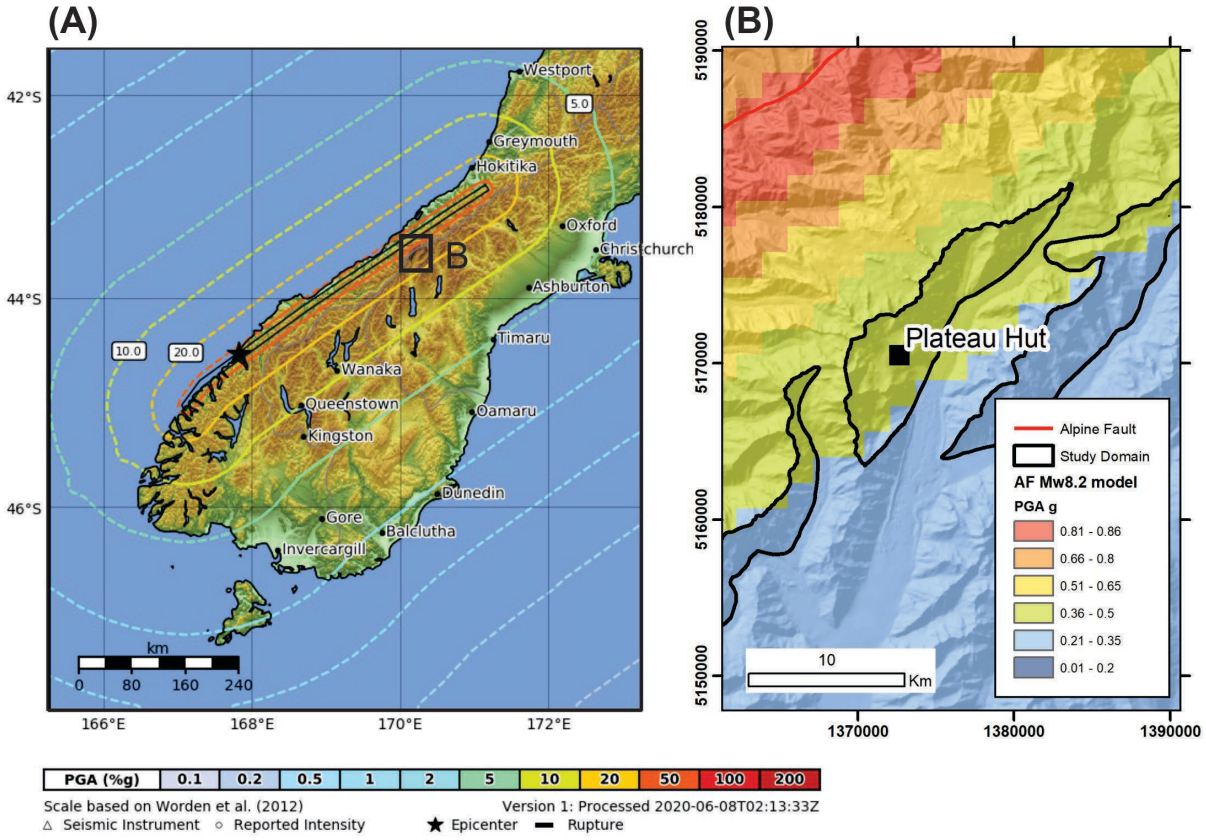

Figure 2.4 ShakeMapNZ simulation of local shaking in subsoils of Class B (rock) from a M_W 8.2 earthquake that ruptures the entire length of the Alpine Fault. (A) Contours of PGA (in %g) output from the ShakeMapNZ program. (B) Detailed view of the PGA grid (values in g) in the vicinity of Plateau Hut.

2.5 Magnitude and Frequency Earthquake-Induced Landslides

The frequency (number) and volume of landslides likely to be generated, given expected levels of ground shaking, need to be estimated in order to calculate earthquake-induced landslide risk. However, as we have yet to experience very strong levels of shaking in the central Southern Alps during post-European time, there is a key uncertainty in the local relationship between landslide density, ground shaking intensity and topography, given (a) the steepness and scale of topography in the central Southern Alps and (b) that numerous landslides already seem to be occurring due to ice-field melting, permafrost degradation and down-wasting of glaciers in the absence of shaking (Allen et al. 2011). Contemporary plate tectonic-related deformation and the passage of seismic waves from distal earthquakes may also have a role in conditioning the stress state of the central Southern Alps rock mass (Cox et al. 2015b; McSaveney et al. 2014, 2015). It is possible that triggering thresholds might be lower, and the number of landslides of a given volume generated at various levels of ground shaking may be higher, than experienced elsewhere.

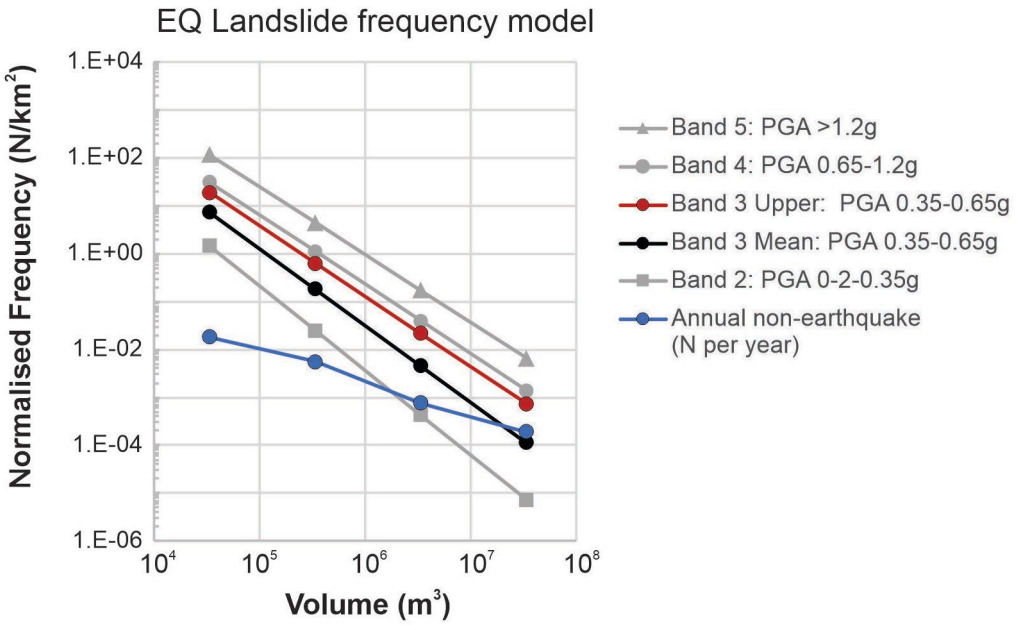

Figure 2.5 Landslide frequency magnitude distribution curves estimated for Band 3 (PGA 0.35–0.65 g) levels of earthquake shaking from historical New Zealand earthquakes. Data are presented as a number per 1 km^2 of source area ≥30°, showing the mean (black circles) and upper (mean + 1 sigma) (red circles) expected values at Grand Plateau for an Alpine Fault earthquake. Calculations for higher and lower levels of shaking (grey) are also shown, together with the annual non-earthquake induced landslides in the 30-year inventory normalised to an annual value (blue, see Figure 2.3). To directly compare between earthquake and non-earthquake landslide production rates in the Southern Alps landscape, the earthquake values need to be normalised over return interval times, which are 249 ± 56 years for the Alpine Fault (Howarth et al. 2021). Points representing volume class ranges are plotted at the geometric mean of each category (following de Vilder and Massey 2020b).

Regardless of this uncertainty, the recommended approach (de Vilder and Massey 2020a, 2020b) is to use scaling relationships from other earthquakes that have triggered landslides in similar topography and bedrock elsewhere, adjusted to local conditions and area/volume relationships. This is possible because landslide frequency / source area distributions have a typical form, whereby the number of landslides decays as an inverse power of landslide area and/or volume (Stark and Hovius 2001; Malamud et al. 2004). Combined distributions of landslides triggered during the 2016 M_W 7.8 Kaikōura, 1968 M_W 7.1 Inangahua and 1929 M_W 7.8 Murchison earthquakes provide seemingly complete records for earthquake-induced landslides in New Zealand (Hancox 2014, 2016; Massey et al. 2018) and are comparable with other international examples (de Vilder and Massey 2020b). These historical New Zealand earthquakes occurred in regions with comparable scales of topography and geology to the central Southern Alps but do have some differences in the ice cover or earthquake mechanisms to an Alpine Fault event.

Inventories of landslides during the historic earthquakes were classified according to levels of ground shaking experienced at each source (de Vilder and Massey 2020b). The number of landslides of different areas were then counted within bands of PGA. Landslide volumes were estimated using an area to volume scaling exponent of 1.17, derived from the mean of Hancox (2014, 2016) and Massey et al. (2018). Power law trends were fitted to parts of the landslide distributions that are thought to be complete (≥10^5 m^3) to obtain equations for the cumulative number of landslides greater than a given volume (following methodology in de Vilder and Massey 2020b). Different curves were generated based on volume/km^2/PGA band for the total area of slopes ≥30°. For a 1 km^2 source area ≥30°, the numbers of landslides that might be expected at different volume classes ≥1000 m^3 and PGA bands, based on de Vilder and Massey (2020b), are listed in Table 2.1 and illustrated in Figure 2.5. The Band 3

(0.35–0.65 g) option seems the most applicable for Alpine Fault earthquake risk analysis at Plateau Hut, encompassing both the 0.36 g PGA predicted by the ShakeMapNZ model (Figure 2.4) and allowing for some degree of directivity effects and/or topographic amplification. These values are used to derive the annual probability of earthquake induced landslides ($P_{H(EIL)}$) in Section 4.2.

Note that Table 2.1 includes all landslides with any chance of reaching Plateau Hut, including 10^4–10^5 m^3 landslides that are shown below (Sections 2.6, 2.7 and 4.2) to have a very small (~1%) possibility of reaching the hut and presenting a hazard. The power law trends fitted from earthquake datasets in de Vilder and Massey (2020b) did not include landslides of this size, as they were deemed to be incomplete (under-sampled) in the earthquake-induced landslide catalogues. The number of small landslides modelled here using fitted equations for a 1 km^2 area appears to be unrealistically high given the area, believed to be an artefact of data extrapolation and the use of logarithmic scales and geometric means. A subjective judgement may need to be applied based on intuition for this 10^4–10^5 m^3 volume class rather than a statistical extrapolation (see Section 4.2).

Table 2.1 Number of landslides of a given volume that might occur per 1 km^2 of source area with slopes ≥30° at different levels of PGA. Two values are given within each PGA band, which are based on the mean and mean +σ (upper) of the Kaikōura, Inangahua and Murchison earthquake-induced landslide inventories (for detailed description of methodology, input data and rationale of bands – see de Vilder and Massey 2020b).

	Number of Landslides of a Given Volume occurring at Various PGA Bands (N_{LS})							
PGA Band	**Band 2 0.2–0.35 g**		**Band 3 0.35–0.65 g**		**Band 4 0.65–1.2 g**		**Band 5 >1.2 g**	
Volume Class (m^3)	**Mean**	**Upper**	**Mean**	**Upper**	**Mean**	**Upper**	**Mean**	**Upper**
10^4–10^5	1.43	4.5	7.4	18.6	31	62	114	359
10^5–10^6	0.025	0.12	0.18	0.63	1.1	2.8	4.4	20.4
10^6–10^7	0.0004	0.0029	0.0046	0.022	0.039	0.129	0.17	1.16
10^7–10^8	0.00001	0.00007	0.00011	0.00073	0.0014	0.0058	0.0065	0.0066

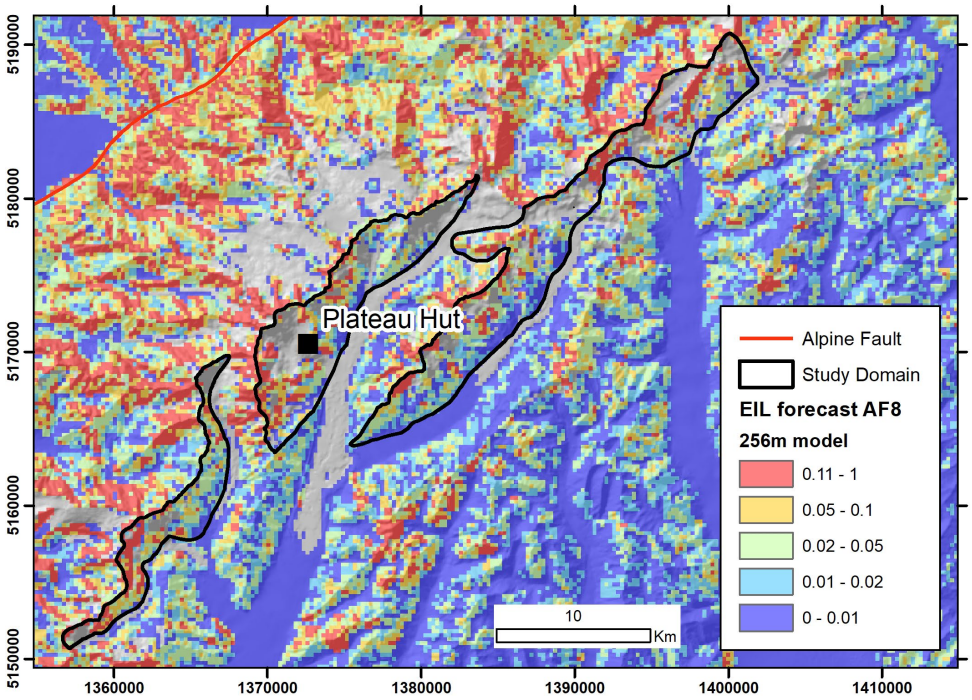

Figure 2.6 Landslide probability map for an Alpine Fault M_W 8.2 earthquake using the EIL forecasting tool and ShakeMapNZ predictions of local ground motion (see Figure 2.4). The probability categories (at 1, 2, 5 and 10% breaks) were selected for being reasonably representative divisions across the 60 km field of view.

As an independent validation, the potential for earthquake-induced landslides at Plateau Hut can be modelled using an EIL (earthquake-induced landslide) forecasting 'tool' (software package) under development at GNS Science (current Version 2.0). The tool aims to provide rapid (5–7 minute) advisory information about the severity and likely location and impacts of landslides following a major earthquake (Massey et al. 2021). Observations of shaking from seismometers are used as input, which are then blended with logistic regression trained on historic earthquake-induced landslide datasets. Version 2.0 uses observations, susceptibility maps and pre-disposing factors for landslides during the M_W 7.8 Kaikōura earthquake, M_W 7.1 1969 Inangahua earthquake and M_W 7.3 1929 Murchison earthquake. Variables used to train the regression models are PGA, proximity to active surface fault traces, local slope relief, slope angle, elevation, slope curvature and geology.

While the tool is designed for fast processing in the immediate aftermath of an earthquake, it can also be run on synthetic PGA models such as output from the ShakeMapNZ Alpine Fault earthquake simulation. A landslide probability map (Figure 2.6) has been created using a M_W 8.2 epicentre at 167.816°E -44.533°S, depth of 6 km, and direct-wave modelled PGA for Class B 'subsoils' (rock). The EIL tool generates an estimate landslide probability (0 to 1, where 1 = landslide occurrence) at a regional scale, intended to show general variations in 'intensity' of landslide occurrence given different levels of shaking. Discretion is required, as the tool is not intended to forecast the probability of landslides over small areas nor the precise location of landslides.

2.6 Landslide Runout

Runout is analysed using the ratio of fall height (H) to horizontal distance (L), whose tangent is commonly proportional to landslide volume (Heim 1932). All 192 rockfalls and rock avalanches within the inventory from the southeast-facing study area (Figure 2.7) are shown in Figure 2.8 as grey dots, with ratios converted to runout angle [in degrees = $\tan^{-1}(H/L)$]. These show a general trend of decreasing runout angle with increasing landslide volume, as expected, but with considerable spread. Factors causing spread and differences in landslide mobility include confined or obstructed runout versus open-slope runout; convex (promoting dispersion and fragmentation) versus concave slopes; and passage across moraine, colluvium or bedrock (less mobile) compared with just snow and ice (more mobile). Some landslides at higher elevation will incorporate snow and ice overlying the failure source area, whereas others may entrain underlying ice or sediment substrate if they are erosive along their runout path.

A subset of 15 rock avalanches local to the Grand Plateau area were selected and analysed independently to decrease some of the variability in runout caused by different snow cover, topography and substrate conditions that are not present locally (Figure 2.7). There were five nearby events that fell from the Main Divide towards the north or west, rather than southwest towards Grand Plateau, which were not included as the snow in the runout path can be affected differently by solar radiation on this aspect (warmed and softened). The Grand Plateau subset forms a much clearer and well-defined negative relationship between runout angle and volume, shown with a linear regression best-fit (blue dots) in Figure 2.8. The number of landslides is sufficient to derive a probability of runout exceedance from the standard error of the regression (McDougall 2017; de Vilder and Massey 2020b), assuming a normal distribution. Probability distributions were calculated using Z-score statistics from the standard error in log (H/L) and the best-fit 50% linear regression on a log (H/L) versus log (volume) plot (Figure 2.9), with the 10% and 90% exceedance relationships shown on the more easily understood Runout Angle versus Volume plot (Figure 2.8, dashed blue lines). These form the basis for determining the spatial probability ($P_{S:H}$) of various-sized landslides impacting on the hut in Sections 4.1 and 4.2.

A different subset of the ‘most mobile’ landslides was also chosen for sensitivity analysis, being five landslides that define the lowermost envelope of the inventory (Figures 2.7 and 2.8; red dots). Landslides with the lowest runout angles have mobility that might have been enhanced, for example, by incorporating a large amount of water or snow within the failing mass. They may even reflect quite distinct mechanisms (e.g. wet debris rather than dry granular flow), but their physics are uncertain as they were not actually observed when they occurred, only recognised afterwards as deposits in aerial or satellite photographs. None of these ‘most mobile’ landslides have occurred at Grand Plateau, so the subset may not be locally applicable. However, they provide a useful worst-possible scenario, generating highest possible risk, as a cross-check in analysis of risk.

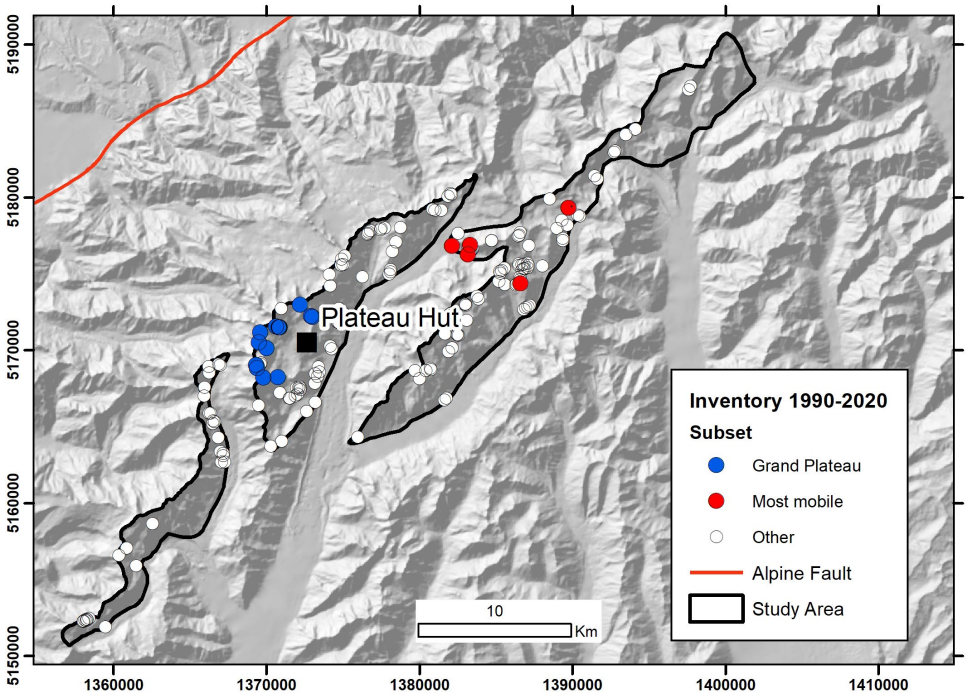

Figure 2.7 Map showing the location of 15 rock avalanches in the Grand Plateau area (blue dots) and five 'most mobile' events (red dots) for comparison with the other 172 landslides (white dots) in the 1990–2020 inventory.

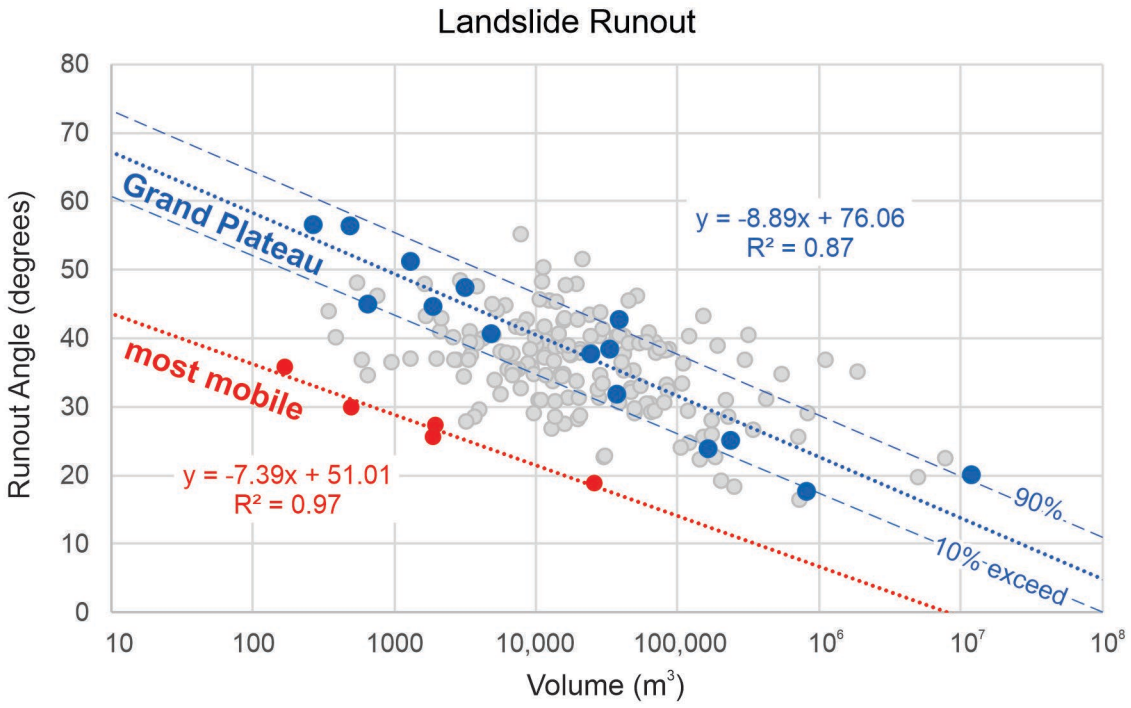

Figure 2.8 Runout plotted as the runout angle of reach (degrees) versus the volume (m^3 scaled logarithmically). Blue markers are 15 landslides in the vicinity of Grand Plateau fitted with a linear regression (dotted blue line), shown together with the approximate position of 10% and 90% runout exceedance probabilities (thin dashed blue lines – see Figure 2.9). Red markers are the five landslides with lowermost runout angles at the base of the data envelope, which represent the most mobile landslides in the 192 landslide inventory (grey markers).

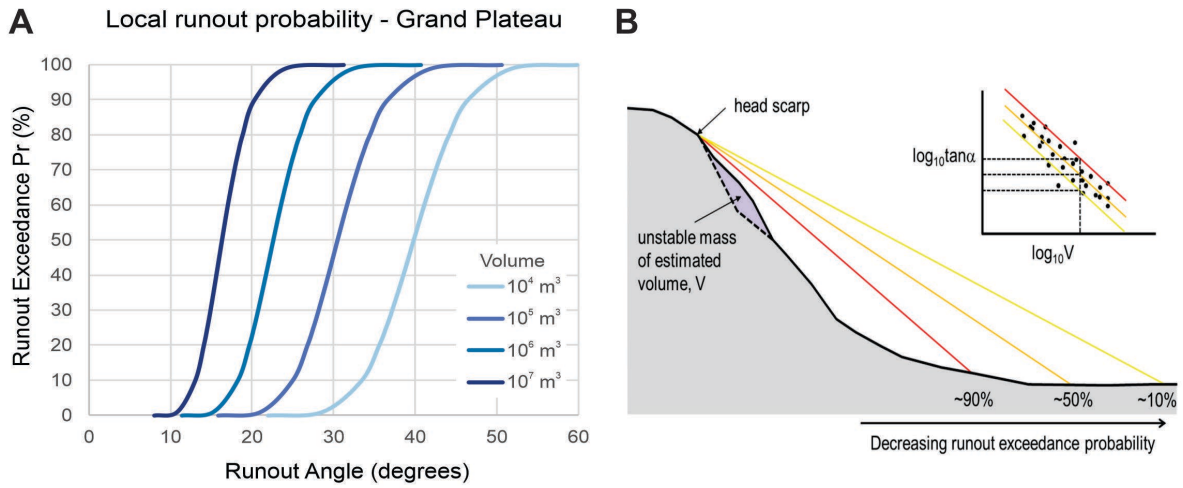

Figure 2.9 Calculation of runout probability based on the scatter of empirical data. (A) Local runout exceedance probability distributions at different volume categories derived from 15 Grand Plateau landslides. (B) Framework of volume versus angle of reach data (from McDougall 2017). Probability distributions were calculated using Z-score statistics from the standard error in log (H/L) and the best-fit 50% linear regression on a log (H/L) versus log (volume) plot, following McDougall (2017) and de Vilder and Massey (2020b).

2.7 Landslide Reach

Angles of reach required from potential source slopes to impact on Plateau Hut have been determined by topographic analysis of the 8 m national DEM (LINZ Data Service 2012) as profile lines along possible runout transects and as grid cell values within 5° increments using the 'Visibility' tool in ArcGIS. The slopes above Grand Plateau that are steep enough to fail (≥30°) are situated at 7–23° reach angles from Plateau Hut (Figure 2.10). Small events are unlikely to be problematic, as they are not capable of runout out across Grand Plateau at <23° sufficient to reach the Plateau Hut. For example, there are few events <10,000 m^3 (that are also under-represented in the inventory Figure 2.3) that can be expected to runout at <35°, assuming the behaviour of other Grand Plateau landslides is followed (Figure 2.8). Probabilities ($P_{S:H}$) assigned to these landslides in risk calculations (see Section 4) are small or zero.

Since Plateau Hut sits on a ridge, locally elevated above parts of Grand Plateau, the path from Silberhorn Ridge to the hut requires about 40 m of uphill climb and from Mt Tasman a 20–30 m gain in elevation. Some degree of protection from avalanches and landslides is also provided to the hut by its location on this ridge, which will likely have been among the factors considered when the first hut was constructed.

The lowermost end of the Mt Haast 2013 and Silberhorn 2020 rock avalanches were both deflected by this local topography (see https://www.youtube.com/watch?v=E28_3uj9K0g; Figures 1.1 and 1.2). The chance of reaching the hut will be reduced for 'smaller' landslides, such as collapse volumes <1 Mm^3 where the sliding mass has been thinned and reaching the end of a decelerating 'flow' as they start to climb uphill. But there are numerous examples in the region of >1,000,000 m^3 avalanches, and a few smaller ones, that have sufficient velocity (e.g. >150 km/hr) to climb up and over a ridge within a few kilometres of their source. Examples include:

- Aoraki / Mount Cook 1991 (12 Mm^3) climbed 100 m over the shoulder of Anzac Peaks and 40 m up the Tasman Moraine wall (dust rising a further 500 m) (Figure 1.2A, McSaveney 2002).

- Hillary Ridge 2014 (900,000 m^3) climbed 40 m up the ridge of Nazomi (and airblast dust 300 m up Hooker wall) (Cox et al. 2015a).
- Vampire 2008 (150,000 m^3) climbed 60 m across the shoulder of Mt Bannie (Cox and Allen 2009).
- Mount Fletcher September 1992 (5 Mm^3) climbed 120 m across a ridge (McSaveney 2002).
- Mount Hutton 2021 (566,000 m^3) had debris climbing 60 m up the Huxley Glacier moraine wall towards Rankin Pass (Cox and Sirguey, unpublished Matariki mapping).

When considering the probability ($P_{S:H}$) that runout would be sufficient to reach the hut, conservative runout angles and probability values have been selected for landslides 10^4–10^6 m^3, but, for those >10^6 m^3, it was assumed that the rise to the hut was insufficient to make a difference to landslide reach or vulnerability of the hut and occupants.

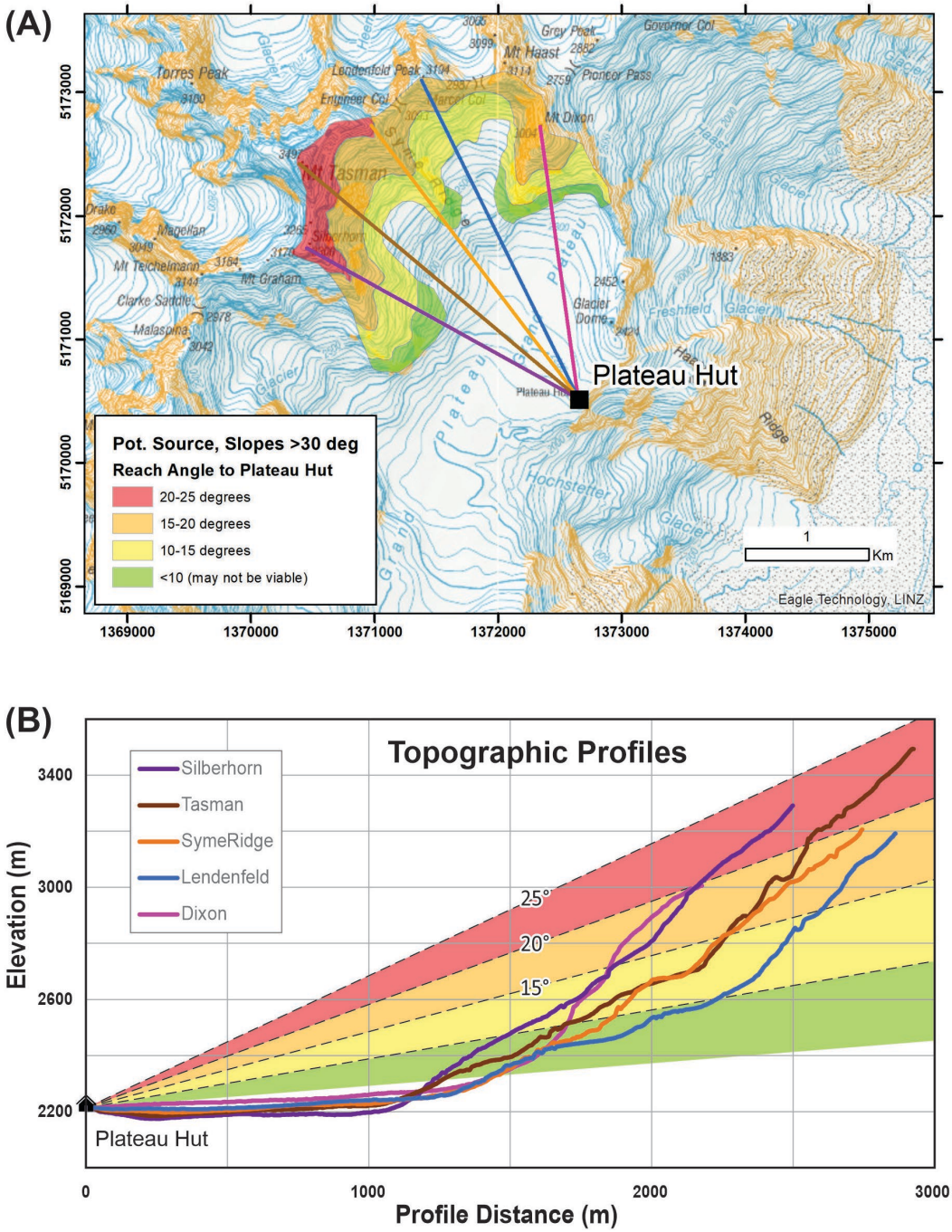

Figure 2.10 The angle of reach between potential landslide (rock avalanche and rockfall) source slopes and Plateau Hut. (A) Map showing 2.6 km^2 of slopes ≥30° coloured according to the angle required to reach the hut. (B) A series of five topographic profile lines along the path from peaks above Grand Plateau to the hut (at a different scale from map but with no vertical exaggeration). Paths from Silberhorn, Tasman or Syme Ridge require a small up-hill climb to reach the hut. The potential source area has been defined from the runout and direction of past avalanches (Figure 1.1). However, not all landslides from the source area will be of size that enables runout sufficient to reach the hut (as indicated by Figure 2.8).

2.8 Ice Avalanches

Ice-cliff collapse and ice avalanches had not been identified as a potentially significant hazard to huts in the AMCNP, or other places in New Zealand, until the possibility was raised in the 2013 hazard assessment (Hancox and Thomson 2013b). Overhanging ice cliffs around 30 to 50 m high develop periodically on hanging glacial slopes above Grand Plateau, waxing and waning over decadal or greater time scales (Figure 1.2C). Small ice-cliff collapses occur every year, but no very large historical events are known to have reached the Plateau Hut site. International examples where very large ice avalanches have been triggered by earthquakes or fallen semi-spontaneously were cited by Hancox and Thomson (2013b). On this basis, they identified the hazard at Plateau Hut. They inferred that a very large (10^6 m^3 or larger) earthquake-induced ice avalanche could occur from the east face of Mt Tasman and runout over the 3 km across Grand Plateau to inundate the hut. Subsequently, the 2015 M_W 7.8 Ghorka earthquake in Nepal triggered many snow and ice avalanches as well as landslides (Kargel et al. 2016), including an ice avalanche from Pumori that ran into Everest Base Camp and killed 22 people, tragically exemplifying the nature of such hazards.

At present, based on satellite imagery and change detection obtained by the Matariki Project, there are three main cliffs on the east face beneath Mt Silberhorn–Mt Tasman–Lendenfeld. The cliffs are up to 200 m wide, with arcuate crevasse fractures reaching 150–250 m upslope that segment glacial ice flow, potentially forming collapsible volumes of 0.6–1.2 Mm^3. Past 'non-earthquake' ice-cliff collapses at Grand Plateau in the past 60 years have been small, without sufficient size or volume to threaten Plateau Hut in the past 60 years (Hancox and Thomson 2013b). Small 'non-triggered' ice collapses are not considered a hazard (i.e. $P_{H(nonEII)}$ = 0 in Equation 1.3). However, based on international experience, it does seem plausible that an earthquake could induce collapse of large volumes of overhanging ice.

There are significant unknowns in quantifying the hazard of avalanche from ice-cliffs at Plateau Hut. Unlike landslides and rock avalanches, there are no New Zealand inventories to characterise the magnitudes and frequencies of collapse, largely because the ice-covered central Southern Alps has not experienced significant earthquake shaking (e.g. at PGA ≥0.2 g levels, Hancox et al. 2002) in the past 300 years. Factors affecting the susceptibility to collapse are likely to vary with the scale of cliffs and presence of crevasses/fractures, as well as temperature, climatic conditions and internal stress of the ice. Historical photographs suggest that there is considerable variation in the development of ice cliffs on the East Face of Tasman over time, such that Hancox and Thomson (2013b) advocated for monitoring of ice-cliff conditions. During an earthquake, different magnitudes of collapse and triggering thresholds will be dependent on the ice cliff size and shape, as well as snow/ice accumulation rate (precipitation), ice velocity and cohesion to underlying bedrock. Cohesion may also be variable within the source area, which potentially spans a transition between permafrost with cold-based ice on the upper slopes and marginal permafrost (or permafrost-free) with wet-based ice on lower slopes (Allen 2009; Allen et al. 2009; Sattler et al. 2016).

Ice avalanche runout is similarly complex and, for the most part, poorly understood. Although there are tools (e.g. RAMMS; https://ramms.slf.ch/ramms/) becoming available for modelling flowing snow avalanches with their associated powder cloud blast hazards (Bartelt et al. 2016), these have not been fully calibrated for avalanches of glacier ice (i.e. blocks with higher density and cohesion). Runout takes on different forms depending on thermomechanical entrainment of ice and snow or melting of ice and snow in the avalanche core (Bartelt et al. 2018). GNS Science has little information to confidently assess whether an ice avalanche mass is capable of reaching the hut (or its probability) or, alternatively, if wind blast from an

associated powder cloud might cause any damage and/or injury to occupants. Possibilities can be rationalised, to a limited extent, by comparing runout against that of equivalent volume rock avalanches.

Key knowledge gaps that need to be answered before there can be full confidence in calculations of hazard and risk from earthquake-induced ice avalanches at Plateau Hut are:

1. What is the probability of an ice-cliff collapse during an earthquake? (Or, alternatively, do earthquake-induced collapses trigger at higher or lower values of PGA than rock avalanches?)
2. How far will ice avalanches runout, and what is the relationship between ice volume and runout angle? (Or, alternatively, do ice avalanches have higher mobility, and runout further, than rock avalanches of an equivalent size?).
3. To what extent is there temporal variability in collapse susceptibility as the glacial ice builds up and then thins on the face over time?
4. Would Plateau Hut provide any protection from a snow avalanche and/or wind blast, such that the vulnerability for an occupant is less than 1?

3.0 CONSEQUENCE

3.1 Exposure

Recent hut-use data and visitor numbers in AMCNP are collected by DOC, aggregated on a monthly basis, including whether parties are guided or non-guided. Due to closure of the huts and travel restrictions caused by COVID-19, numbers for 2020 and 2021 were significantly different from the prior three years. The statistics requested by DOC (Don Bogie, pers. comm.) to be used in risk calculations for Plateau Hut are based on 2019 rather than the more recent data (Table 3.1). These figures are used to calculate temporal spatial probability ($P_{T:S}$) of people, or multiple people, being present at the hut.

Table 3.1 Visitor statistics for Plateau Hut from 2019, selected by Don Bogie / DOC for use in risk calculations.

Plateau Hut (33 Beds)	Details	Proportion
Total bed nights 2019	1133	N/A
Total visitors	483	N/A
Average hours per day of visit, assuming visitors go out climbing/ skiing during the day beyond the hazard footprint (time inferred from experience; not measured)	14	0.583 per day
Nights occupied	120	0.329 per year
Proportion of year hut occupied (N≥1)	14/24 hours and 120 days	0.192 per year
Proportion of year at least 5 people present (N≥5)	Estimated to be 80% of occupied time (96 days)	0.153 per year
Proportion of year at least 30 people present (N≥30)	Estimated at 50% of time during two busy months	0.028 per year

3.2 Vulnerability

There is little available information on the vulnerability of people within mountain huts or small buildings when impacted by a landslide, nor how the design and foundations of Plateau Hut might perform under such an impact. Accordingly, different values of vulnerability for people inside the hut have to be assigned using ‘expert opinion’. Here we follow recommendations of de Vilder and Massey (2020b), drawn from other international studies, assigning values based on assumptions about how vulnerability may vary according to different volumes of the landslide, allowing for spread and changes in velocity during the runout (Table 3.2). It has also been assumed that there would be little or no warning for occupants of the hut or, if there was warning, there would be insufficient time to escape the path of any rock avalanche that reaches the hut.

Table 3.2 Vulnerability values used in risk calculations that allow for spread and changes in velocity during the runout, together with other assumptions around impact of different volumes of landslides on Plateau Hut. Values have been assigned following recommendations in de Vilder and Massey (2020b).

Volume Category	Assumption	Vulnerability (V)
10^2–10^3 m^3	Minor debris strikes hut; virtually no danger	0.05
10^3–10^4 m^3	Hut inundated but person not buried; high chance of survival	0.1
10^4–10^5 m^3	Hut inundated, some protection; chance of survival	0.2
10^5–10^6 m^3	Hut inundated and partially collapsed; survival possible	0.5
10^6–10^7 m^3	Building inundated and collapses; survival unlikely	0.9
≥10^7 m^3	High velocity impact and/or hut swept from site; death almost certain	1.0

4.0 RISK ESTIMATION

4.1 Non-Earthquake Landslide Risk

An initial estimate of LPR from non-earthquake landslides $P_{LPR(nonEQL)}$ = 1.83 x 10^{-3} has been derived in Table 4.1, based on Equation 1.1. Calculations used the 192 landslides within the landslide inventory to derive frequency of different landslide volume classes from the 172 km^2 of ≥30° slopes within the southeast-facing study area, normalised over a 30-year period (Section 2.3). This provides the annual probability, $P_{H(nonEQL)}$, of landslides at different sizes from the 2.6 km^2 of potential source slopes above Grand Plateau. The probability that the runout is sufficient to reach Plateau Hut, $P_{S:H}$, has been derived from the linear regression of runout from the subset of 15 local landslides in the vicinity of Grand Plateau (Figure 2.8) and the probabilities that runout from these landslides (Figures 2.8 and 2.9) will exceed the average reach to Plateau Hut of ≥30° slopes within the 2.6 km^2 source area, based on the runout Z-score statistics (see Sections 2.6 and 2.7). Vulnerability values, V, have been assigned based on other studies (Table 3.2). Assuming that the average time spent at the hut is 14/24 hours (Table 3.1), Equation 1.2 can be used to estimate an individual visitor risk per day per trip at $P_{IRPD(nonEQL)}$ = 2.93 x 10^{-6}.

To test the sensitivity and importance of being more precise with runout, and values of $P_{S:H}$ in particular, the initial estimate of risk was repeated but with the source area divided into two. This enables calculations to include more precise runout angle and differences in $P_{S:H}$ associated with source elevation. Data were subdivided into the 1.35 km^2 of upper slopes, where the reach angle to Plateau Hut is ≥15–23° (orange and red zone in Figure 2.10), and 1.26 km^2 of lower slopes, where the angle of reach is <15° (yellow and green zones in Figure 2.10). Assuming independence of hazardous events from these areas, the hazard probabilities from the two areas was then summed for an overall hazard (bottom row, Table 4.2). This 'Sensitivity analysis 1' suggests a slightly higher risk for all non-earthquake landslides at $P_{IRPD(nonEQL-S1)}$ = 4.65 x 10^{-6} (Table 4.2) compared with 2.93 x 10^{-6} (Table 4.1).

As a separate cross-check, the analysis was repeated using the most mobile landslides in the study area (Sensitivity analysis 2; see Figures 2.7 and 2.8, red dots). Although no such landslides have been observed at Grand Plateau, they provide a worst-case test of runout possibility. Were all non-earthquake landslides to have such mobility, including the largest rock avalanches, the risk at the hut might potentially be as high as $P_{IRPD(nonEQL-S2)}$ = 1.46 x 10^{-5} (Table 4.3).

Table 4.1 Non-earthquake landslide risk analysis for Plateau Hut. The N/yr and annual event probability ($P_{H\text{-}nonEQ}L$) columns are based on all 192 events in the study area inventory. The probability $P_{S:H}$, that runout is sufficient to reach the hut, is calculated from standard errors of runout versus volume observed in the subset of 15 Grand Plateau landslides, using runout exceedance probability given the <25° angle of reach between the source area and the hut (see, for example, the 10% probability exceedance line in Figure 2.8).

Volume Class (m^3)	Number of Events in Study Area (172 km^2, ≥30°) in 30 Years (1990–2020)	Annual Probability of Event from ≥30° Slopes (2.6 km^2) above Plateau	Equivalent Return Interval (Years)	Probability Runout Sufficient to Reach Hut	Probability Person Killed if Present	Annual Probability of Death if Present	Individual Risk per Day
	N/yr	$P_{H\ (nonEQL)}$	RI	$P_{S:H}$	V	P_{LPR} (nonEQL)	P_{IRPD} (nonEQL)
10^2–10^3	12	0.0061	164	0	0.05	0	0
10^3–10^4	53	0.0269	37	0	0.1	0	0
10^4–10^5	93	0.0472	21	0.01	0.2	9.44 E-5	1.51 E-7
10^5–10^6	29	0.0147	68	0.05	0.5	3.68 E-4	5.88 E-7
10^6–10^7	4	0.0020	492	0.5	0.9	9.14 E-4	1.46 E-6
≥10^7	1	0.0005	1970	0.9	1	4.57 E-4	7.30 E-7
Total	**192**	**0.0975**				**1.83 E-3**	**2.93 E-6**

Table 4.2 Sensitivity analysis 1 for non-earthquake landslide risk at Plateau Hut. The source area has been divided approximately in two and risk calculated separately for lower slopes (green), where the angle of reach to Plateau Hut is <15°, and upper slopes (blue), where the angle is between 15° and 25°. The probability $P_{S:H}$, that runout is sufficient to reach the hut, is based on standard errors of runout versus volume observed in the 15 Grand Plateau landslides and the runout exceedance probability given various angles of reach to the hut (see Figure 2.8).

Volume Class (m^3)	Annual Probability of Event from Slopes above Plateau Hut Lower 1.29 km^2, <15° Reach Upper 1.35 km^2, 15–23° Reach	Probability Runout Sufficient to Reach Hut	Probability Person Killed if Present	Annual Probability of Death if Present	Individual Risk per Day
	$P_{H\ (nonEQL)}$	$P_{S:H}$	V	$P_{LPR(nonEQL)}$	$P_{IRPD(nonEQL)}$
10^2–10^3	0.0030 0.0031	0 0	0.05	0 0	0 0
10^3–10^4	0.0131 0.0138	0 0.001	0.1	0 6.9 E-7	0 1.10 E-9
10^4–10^5	0.0231 0.0242	0 0.05	0.2	0 2.4 E-4	0 3.86 E-7
10^5–10^6	0.0072 0.0075	0.01 0.3	0.5	3.6 E-5 1.1 E-3	5.74 E-8 1.81 E-6
10^6–10^7	0.0010 0.0010	0.2 0.9	0.9	1.8 E-4 8.4 E-4	2.85 E-7 1.34 E-6
≥10^7	0.0002 0.0003	0.9 1.0	1	2.2 E-4 2.6 E-4	3.56 E-6 4.15 E-7
Total	**0.0975**			**2.9 E-3**	**4.65 E-6**

Table 4.3 Sensitivity analysis 2 for non-earthquake landslide risk at Plateau Hut. As for Table 4.2, but where the probability $P_{(S:H)}$, that runout is sufficient to reach the hut, is based on the five most mobile landslides observed in the study area (see Figure 2.8). These have the lowermost runout angles in the dataset, from 1990 to 2020, but were not observed in the vicinity of Grand Plateau. They represent a worst-possible case with highest possible risk in which rock avalanche mobility might be enhanced, for example, by incorporating a large amount of ice and snow within the failing mass. The sensitivity analysis highlights the importance of understanding local runout characteristics.

Volume Class (m^3)	Annual Probability of Event from Slopes above Plateau Hut Lower 1.29 km^2, <15° Reach Upper 1.35 km^2, 15–23° Reach	Probability Runout Sufficient to Reach Hut	Probability Person Killed if Present	Annual Probability of Death if Present	Individual Risk per Day
	$P_{H\ (nonEQL)}$	$P_{S:H}$	V	$P_{LPR(nonEQL)}$	$P_{IRPD(nonEQL)}$
10^2–10^3	0.0030 0.0031	0 0	0.05	0 0	0 0
10^3–10^4	0.0131 0.0138	0 0.05	0.1	0 3.44 E-5	0 5.50 E-8
10^4–10^5	0.0231 0.0242	0.05 0.5	0.2	2.31 E-4 2.42 E-3	3.68 E-7 3.86 E-6
10^5–10^6	0.0072 0.0075	0.1 1	0.5	3.59 E-4 3.77 E-3	5.74 E-7 6.02 E-6
10^6–10^7	0.0010 0.0010	1 1	0.9	8.92 E-4 9.35 E-4	1.43 E-6 1.49 E-6
≥10^7	0.0002 0.0003	1 1	1	2.48 E-4 2.6 E-4	3.96 E-7 4.15 E-7
Total	**0.0975**			**9.14 E-3**	**1.46 E-5**

4.2 Earthquake-Induced Landslide Risk

Expected numbers of landslides during an Alpine Fault earthquake event have been determined assuming that the shaking will correspond to Band 3 PGA (Figure 2.5, Table 2.1), scaled to the 2.63 km^2 source area of slopes ≥30° above Plateau Hut (Table 4.4, N values). Only the range of landslides realistically expected to be hazardous to Plateau Hut are listed, but the number for smallest landslides calculated for the 10^4–10^5 m^3 volume category appears unrealistically large (see Section 2.5) and so can be expected to generate high (conservative) values of risk. The probability that runout will be sufficient to reach the hut ($P_{S:H}$) was derived from runout of the non-earthquake landslides recorded for 15 landslides in the Grand Plateau area from 1990 to 2020 (Sections 2.6 and 2.7). As there remains uncertainty from fitting trends in earthquake-induced landslide datasets, in addition to the possible variation in shaking and topographic amplification of PGA that may occur, the number of events (N) has been provided as mean and upper (mean + 1 sigma) values.

Table 4.4 Alpine Fault earthquake landslide risk analysis for Plateau Hut. The number of landslides, N, uses scaled values per km^2 at PGA 0.35–0.65 g (Band 3), with both mean and mean +σ (upper = *red*) values listed here from the combined Kaikōura, Inangahua and Murchison earthquake-induced landslide inventories. See text for discussion over possible over-estimation of numbers of 10^4–10^5 m^3 landslides. Note that the red values in *italics* are 'alternative' values and, unlike Tables 4.2 and 4.3, are not 'additional' to the risk.

Volume Class (m^3)	Number of Events from 2.6 km^2 Source Area Mean (Upper) at PGA Band 3 (0.35–0.65 g)	Probability Runout Sufficient to Reach Hut	Probability Person Killed if Present	Probability of Death in a Band 3 Earthquake Event	Annual Probability of Death if Present	Individual Risk per Day
	N	$P_{S:H}$	V	P_{LOL}	$P_{LPR\ (EIL)}$	$P_{IRPD\ (EIL)}$
10^4–10^5	? 19.4 *? 48.9*	0.01	0.2	3.87 E-2 *9.78 E-2*	Hazards are from the same causative earthquake event and not independent, so theory of unimodal bounds and de Morgan's rule is used (see de Vilder and Massey 2020a) to calculate an upper bound conditional probability before applying a 0.015 annual probability.	
10^5–10^6	0.48 *1.66*	0.05	0.5	1.20 E-2 *4.16 E-2*		
10^6–10^7	0.012 *0.057*	0.5	0.9	5.39 E-3 *2.55 E-2*		
10^7–10^8	0.0003 *0.0019*	0.9	1	2.69 E-4 *1.73 E-2*		
Total				**5.57 E-2** **1.59 E-1**	**8.35 E-4** **2.38 E-3**	**1.33 E-6** **3.80 E-6**

At shaking within the 0.35–0.65 g range expected from an Alpine Fault earthquake, there are a range of possible landslide sizes that could impact on the hut, but only one can be expected to cause loss of life. Because the volume classes do not represent independent hazards, an upper-bound conditional probability has been calculated using the theory of unimodal bounds and de Morgan's rule to estimate the combined hazard from different landslide volumes (de Vilder and Massey 2020a). The conditional probability of loss of life (P_{LOL}) was estimated before applying the 0.015 annual frequency of an Alpine Fault event to derive LPR $P_{LPR\ (EIL)}$ = 8.35 x 10^{-4} or 2.38 x 10^{-3} and individual risk per day $P_{IRPD\ (EIL)}$ = 1.33 or 3.80 x 10^{-6} (Table 4.4) for earthquake-induced landslides.

It was noted previously (Section 2.6) that the modelled number of 10^4–10^5 m^3 landslides triggered from the source area during an earthquake, based on fitted curves from other earthquakes, appears to be intuitively too high. Nearly 20 landslides of this volume from a 2.6 km^2 area is a lot, especially given that much of the area is covered in ice. But, because the probability of smaller landslides reaching the hut is low, it has a limited effect on the total modelled risk. For example, if the number is reduced, say to selected judgment values of N = 2 (mean) or N = 4 (upper), the total risk would be less than half that calculated in Table 4.4 but not different by an order of magnitude (e.g. values at N = 2 and 4 generate $P_{LPR\ (EIL)}$ = 3.23 x 10^{-4} to 1.13 x 10^{-3} and individual risk per day $P_{IRPD\ (EIL)}$ = 5.17 x 10^{-7} to 1.80 x 10^{-6}). However, as the actual number of small landslides is unknown, it seems appropriate and perhaps preferable to adopt the more conservative (higher) risk values in Table 4.4.

The estimates of risk for earthquake-induced landslides in Table 4.4 equate to a somewhat higher level of risk than estimated by Hancox and Thomson (2013b). This is principally because calculations here adopt an annual probability for a future Alpine Fault earthquake to be 75% in the next 50 years (from Howarth et al. 2021) rather than an annual average normalised over the entire recurrence interval of an earthquake cycle (Hancox and Thomson 2013b used 329 years).

As an independent sensitivity test (Sensitivity test 3), when the modelled M_W 8.2 Alpine Fault earthquake in ShakeMapNZ (Figure 2.4) is input into the EIL forecasting tool, a set of landslide probabilities can be derived (Figure 2.6). The mean landslide probability is 0.025 using a 32 m grid cell model, or 0.125 with 512 m cells, within the southeast-facing study area with ≥30° slopes (Figure 2.6). Applying the '75% chance of an earthquake in next 50 years' probability, the forecasting tool provides indicative annual earthquake-induced landslide P_H probabilities of 3.75×10^{-4} or 1.88×10^{-3}. If we assume that 50–90% of landslides in the source area above Plateau will be sufficiently large and mobile to reach the hut (i.e. $P_{S:H}$ =0.5–0.9), where vulnerability will be V=1, values of $P_{LPR(EIL\text{-}S3)}$ would range between 1.88×10^{-4} and 1.69×10^{-3}, with daily risk for 14/24-hour exposure at $P_{IRPD(EIL\text{-}S3)} = 1.80 \times 10^{-6}$ to 2.70×10^{-6}. These values are comparable to those in Table 4.4 ($P_{IRPD(EIL)}$ range 1.33 to 3.80×10^{-6}), which is not entirely unexpected as the two calculations both ultimately rely on the same original historic earthquake datasets. The EIL forecasting tool provides an independent validation of the risk calculation methodology.

4.3 Ice Avalanche Risk

The annual probability of death from a large earthquake-induced ice avalanche was estimated at 1.14×10^{-3} (Hancox and Thomson 2013b), which was the most significant geological hazard that dominated total risk at Plateau Hut. Their calculation was based on: (i) the return period of an Alpine fault earthquake (at that time thought to have a 329 year recurrence interval[4]), (ii) the assumption that a collapse was 100% probable (inevitable) in an earthquake, (iii) that runout had a 75% probability of being sufficient to reach the hut, (iv) there was 50% occupancy at Plateau Hut (giving a temporal spatial probability during the year but assuming 24-hour presence) and (v) that individuals were totally vulnerable in an event (V = 1).

Using the same approach as the Hancox and Thomson (2013b) assessment, updated with a 75% probability of an Alpine Fault event in the next 50 years (P_H = 0.015), using $P_{S:H}$ = 0.75, V = 1 and occupation at 120 nights (0.329 per year) (from Table 3.1), the annual probability of death from an earthquake-induced icefall would be $P_{LPR(EII)} = 3.70 \times 10^{-3}$. Equivalent individual risk per day is $P_{IRPD(EII)} = 5.91 \times 10^{-6}$ but, for reasons outlined below, this number appears potentially high.

Firstly, as well as temporal variation in susceptibility of the glacial ice, there will be spatial variations in probability such that shaking should not be expected to trigger ice-cliff collapses from the slope in 100% of earthquakes. On this basis, the annual probability of a collapse event $P_{H(EII)}$ seems likely to be only a proportion of the annual probability of that earthquake, and the $P_{IRPD(EII)}$ cited above could over-estimate risk by an order of magnitude. Secondly, there is also little information from which the $P_{(S:H)}$ '75% probability that a 10^6 m^3 ice-cliff collapse would reach the hut' assumed by Hancox and Thomson (2013b) can be validated or tested.

4 Only the 329-year return period for an Alpine Fault earthquake was used by Hancox and Thompson (2013), although at the time it was calculated to have ~30% chance of occurrence in the next 50 years. Alpine Fault earthquakes are now thought to recur at 249 ± 58 years (1σ), with a 75% chance in the 50 years (Howarth et al. 2021).

In comparison, a 10^6 m^3 rock avalanche has $P_{S:H}$ between 1% and 70% chance of runout at the 15–25° reach angles required to reach Plateau Hut from the same elevation as the ice cliffs (from Figures 2.8 and 2.10).

As an alternate way of assessing the problem, yet still making assumptions due to significant knowledge gaps and without any real supporting data, the probability of an earthquake triggering a 10^6 m^3 ice avalanche might be considered to be similar to the triggering of a smaller rock avalanche. Combining annual probabilities for an earthquake-induced rock avalanche in the 10^5–10^6 m^3 category $P_{H(EII)} = P_{H(EIL)} = 0.0072$ (or upper 0.025) from Table 4.4, with runout $P_{S:H}$ = 0.5–0.75, occupant vulnerability V = 1, yields a 14/24-hour $P_{IRPD(EII)}$ ranging from 5.75 x 10^{-6} to 2.99 x 10^{-5}. Importantly, these calculations also suggest that there may be higher risk from ice avalanches than either earthquake-induced landslides ($P_{IRPD(EIL)}$ = 1.35 x 10^{-6} to 3.99 x 10^{-6}; Table 4.4) or non-earthquake induced landslides ($P_{IRPD(nonEQL)}$ = 2.93 x 10^{-6}; Table 4.1).

Although there are significant knowledge gaps (Section 2.8), it is rational that the hazard and risk from earthquake-induced ice-cliff collapse could be significant, potentially at levels equivalent to, or even at higher probability, than rock avalanches during the same event. At a qualitative level, ice avalanches potentially contribute $P_{LPR(EII)}$ = 3.7 x 10^{-3} or $P_{IRPD(EII)}$ = 6 x 10^{-6} toward the total risk, but this will not be independent from the rock avalanche risk. However, without knowing exactly what factors control susceptibility, how an ice avalanche may runout and to what extent the susceptibility varies as glacial ice waxes and wanes over time, the epistemic uncertainty is high. The possibility that the ice cliffs will not always collapse during an Alpine Fault earthquake, or an ice avalanche will not always reach the hut, means that the ice avalanche risk calculated here is likely a maximum value. More work is required to quantify the earthquake-induced ice avalanche hazard if the risk estimation is to reach the 'advanced level' of DOC requirements (cf. de Vilder and Massey 2020a, 2020b).

4.4 Total Individual Risk

Risk has been quantified above for both non-earthquake- and earthquake-induced landslides, together with some sensitivity analysis, in light of new information on both the present rate of collapses in AMCNP, runout and probability of an Alpine Fault earthquake. The principal metrics presented above are local personal risk, P_{LPR}, and individual risk per day per trip, P_{IRPD}, – being the daily probability of death by landslide for a theoretical imaginary person present at the hut 58% of the time (14/24 hours each day). Risk estimates, based on calculations, judgement and ranges from sensitivity testing, are summarised in Table 4.5. Non-earthquake-induced landslides appear to present slightly higher levels of risk than Alpine Fault earthquake-induced landslides.

Additional risk from earthquake-induced ice avalanches is more poorly constrained and contains considerable epistemic uncertainties. Values have been re-calculated in the context of the new information on Alpine Fault earthquake probability, but there is lower confidence in the risk estimates than those determined for landslides. Levels of risk are rationalised as maxima and provided with caveats on the lack of data on ice-cliff collapse and triggering during earthquakes, or large ice avalanche runout. New research is needed before the ice avalanche component of risk at Plateau Hut can be quantified with full confidence.

The annual probability of death, for a theoretical imaginary person present at the hut 100% of the time (24 hours each day), is within or below a range of ΣP_{LPR} = 6.0 to 9.0 x 10^{-3}. The individual risk per day per trip P_{IRPD} metric is based on the proportion of a 24-hour day that people are exposed to a hazard, which has been inferred by DOC to be on average 14 hours per day (Table 3.1), as few visitors will spend 24 hours of the day in the hut. The daily

risk to an individual is calculated from all of these component hazards (using Equations 1.3 and 1.4) at ΣP_{IRPD} = 1.0 to 1.5 x 10^{-5} (Figure 4.1).

The risk at Plateau Hut can be considered in context with selected popular tourist activities in New Zealand (e.g. cycling, walking, rafting, jet boating and parachute and bungy jumping, as in Massey et al. [2019]). Risk of staying at the hut is significantly lower than risk during a climb of Aoraki / Mount Cook (ranging between 1.3 x 10^{-4} to 6.5 x 10^{-3}, Massey et al. [2019]). Individual risk per day at the hut is comparable with fatality rates per hour of flight for helicopters carrying out commercial passenger transport flights in New Zealand, calculated at between 4.5 x 10^{-6} and 1.5 x 10^{-5} by Taig and McSaveney (2015) using Civil Aviation Authority and Transport Accident Investigation Commission data of 1998–2013 air travel and fatal air accidents in New Zealand (also provided in Massey et al. [2019]). Given that many visitors arrive or leave by helicopter (two-way flying time of 20–30 minutes), while others climb to or from the hut (a tricky 8–10 hours from the road end), visitors may well have exposed themselves to equivalent (or higher) risk during the journey to and from the hut as during their stay.

Two components of the Plateau Hut risk, non-earthquake-induced landslides (making ~28–32% of total risk) and earthquake-induced landslides (~13–27% of total) have been quantified with a relatively high degree of confidence, but with an assumption that runout mobility will match the 15 rock avalanches observed in the Grand Plateau area during the past 30 years. There have been other more mobile landslides observed elsewhere in AMCNP, generally at lower elevations where precipitation more commonly occurs as rain rather than snow. It is conceivable that changing precipitation or ice-melt through climate change could, at some time, cause landslides at Grand Plateau to become wetter and therefore more mobile. Should any future rock avalanches develop the ‘most mobile’ runout characteristics, the total daily risk at Plateau Hut could potentially be as much as three times higher at ‘worst possible’ $\Sigma P_{(IRPD)}$ = 2.5 x 10^{-5}. Such a level of risk is not yet considered viable but needs to be constantly assessed.

As Plateau Hut does not have any resident warden or staff, there are relatively few people who spend extended periods of time at the hut. Mountain guides may have the greatest exposure to risk, for whom the annual individual fatality risk (AIFR) may be a more useful and appropriate risk metric (de Vilder and Massey 2020a). The AIFR metric has not been calculated here, as data on the most exposed users is not readily available, but it is simply the total risk experienced over one full year of working from the hut, being the individual risk per day times the number of days visiting the hut.

Table 4.5 Summary of individual risk calculations and metrics with values rounded to one significant figure.

Hazard	Annual Probability of Death by Landslide for a Theoretical Imaginary Person Present at the Hut 100% of the Time	Daily Probability of Death by Landslide for a Theoretical Imaginary Person Present at the Hut 58% of the Time (14/24 hours each day)	Comment
	P_{LPR}	P_{IRPD}	
Non-earthquake landslides (nonEQL)	1.8 to 2.9 x 10^{-3} worst case 9.1 x 10^{-3}	2.9 to 4.7 x 10^{-6} worst case 1.5 x 10^{-5}	Rock avalanches and major rockfalls. Runout based on 15 local events, with 'worst case' based on five most-mobile runouts seen elsewhere in AMCNP.
Earthquake-induced landslide (EIL)	8.4 x 10^{-4} to 2.4 x 10^{-3}	1.3 to 3.8 x 10^{-6}	Rock avalanches and/or major rockfalls. Numbers based on experience from other New Zealand earthquakes. Possible over-estimation for small landslides (10^4–10^5 m^3) results in conservative values.
Earthquake-induced ice avalanche (EII)	Rationalised at 3.7 x 10^{-3} maximum	Rationalised at 6 x 10^{-6} maximum	No data on chance of earthquake triggering ice-cliff collapse or large ice avalanche runout reaching the hut. Quoted value is therefore a maximum.
Total All hazards	ΣPLPR = 6.3 to 9.0 x 10^{-3} worst possible 1.5 x 10^{-2}	ΣPIRPD = 1.0 to 1.5 x 10^{-5} worst possible 2.5 x 10^{-5}	Apply upper-bound conditional probability for earthquake-induced hazards. 'Worst possible' requires a future change in local landslide runout characteristics.

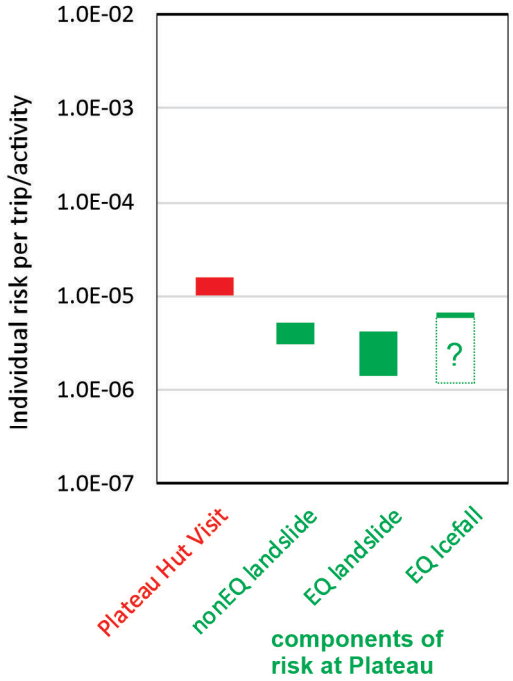

Figure 4.1 Individual fatality risk per day during a Plateau Hut visit (red = range of ΣP_{IRPD}) and three hazard components that make up this risk (green). Risk from earthquake-induced icefall and ice avalanche has a high degree of uncertainty and is considered a maximum.

4.5 Societal Risk

A basic-level societal or group risk has been calculated based on the relationship between the frequency of occurrence of any landslide or ice avalanche and the number of people killed if that hazard were to occur. Periods when there are N≥5 or N≥30 people staying at the hut have been estimated, based on information supplied by DOC (Table 3.1). Based on 2019 statistics, there are ≥5 people for approximately 80% of the 120 days per year that the hut is occupied and ≥30 people for approximately 50% of the time that the hut is occupied during the two busiest months of November and December (when the hut is occupied an average of 18 days). Associated risks of multiple fatalities are therefore:

- Annual risk ≥5 killed $\Sigma P_{SOC\ (N\geq5)}$ = $\Sigma P_{(LPR)}$ x 80% x 120/365.25 days x 14/24 hours
  = 9.7×10^{-4} to 1.4×10^{-3}
- Annual risk ≥30 killed $\Sigma P_{\ SOC(N\geq30)}$ = $\Sigma P_{(LPR)}$ x 50% x (18 x 2)/365.25 x 14/24 hours
  = 1.8 to 2.6×10^{-4}

In other words, there is about five times less chance of ≥30 than ≥5 fatalities. The method adopted here produces a societal risk that is simplified compared some other studies (e.g. Strouth and McDougall 2021). It includes all possible sized landslides or ice avalanches rather than a series of specific scenarios.

The societal risks at Plateau Hut, calculated above, have been used to generate an f/N curve depicting the expected annual frequency of occurrence (f) of a given number (N) of deaths (or the expected number of deaths of a given annual frequency). Risks are lower than those from past New Zealand earthquakes, or storm and flood events, that have killed multiple people (Figure 4.2).

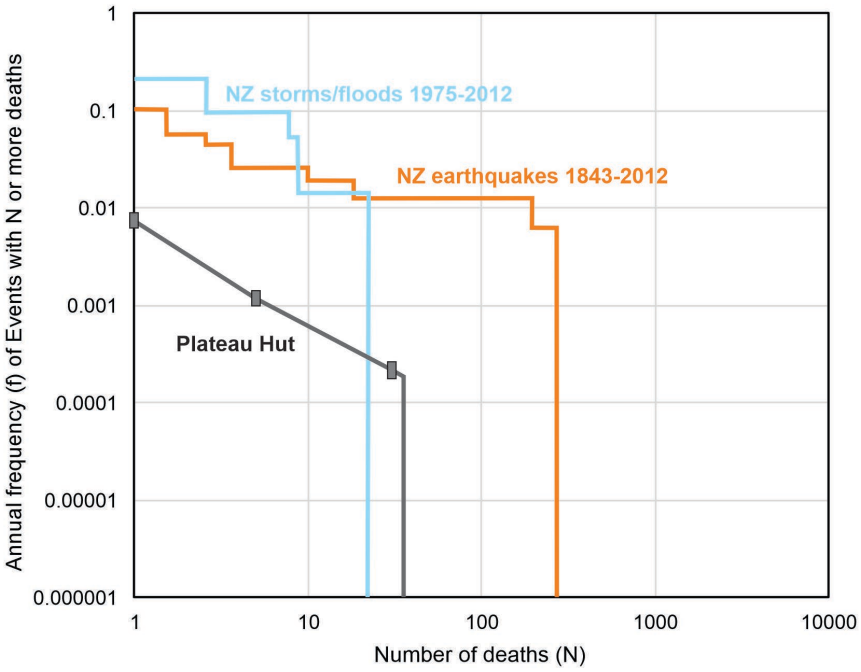

Figure 4.2 Plateau Hut visitor societal risk in terms of a chart of frequency (f) of an event causing a number (N) or more deaths. Multiple fatalities from New Zealand earthquake and storm/flood events are shown for comparison (after Massey et al. 2019).

5.0 CONCLUSIONS

This report updates an earlier assessment of hazard and risk at Plateau Hut in the Aoraki / Mount Cook National Park, by taking into account new information on the frequency and occurrence of local landslides, the probability of an Alpine Fault earthquake and data and modelling of earthquake-induced landslides elsewhere in New Zealand. It follows standardised guidelines for natural hazard risk analysis on public conservation lands and waters (de Vilder and Massey 2020a, 2020b).

An inventory of landslide sources and collapse volumes was developed from 192 rock avalanche and large rockfall events that occurred between 1990 and 2020 in a 219 km^2 study area. Runout models were developed from a subset of 15 that occurred locally in the Grand Plateau area.

Risk has been quantified for both non-earthquake- and earthquake-induced landslides in light of the above information, together with some sensitivity analysis. The principal metrics presented are the local personal risk, P_{LPR}, of death each year and the individual risk per day per trip, P_{IRPD}, as the daily probability of death by landslide for a theoretical imaginary person present at the hut 58% of the time (14/24 hours each day). Calculated values, rounded to one significant figure, are:

- Non-earthquake-induced landslides $P_{IRPD\ (nonEQ)} = 2.9$ to 4.7×10^{-6} (worst case 1.5×10^{-5})
- Earthquake-induced landslides $P_{IRPD\ (EIL)} = 1.3$ to 3.8×10^{-6}
- Earthquake-induced ice avalanche $P_{IRPD\ (EII\ )} = 6 \times 10^{-6}$ (likely a maximum)
- Total Daily Risk $\Sigma P_{IRPD} = 1.0$ to 1.5×10^{-5}.

However, there is little information on ice-cliff collapse and triggering during earthquakes or large ice avalanche runout, so this component of risk is considered to be ‘inferred’ rather than fully quantified. The possibility that ice cliffs will not always collapse during an Alpine Fault earthquake, or that an ice avalanche will not always reach the hut, means that the ice avalanche risk value presented is likely a maximum and therefore conservative. Further work to understand ice avalanches can be expected to decrease total risk values at the hut. Societal Risk of multiple fatalities at Plateau Hut has been determined on the basis of 2019 occupancy data selected by DOC. The annual risk of death of ≥5 people is $\Sigma P_{SOC\ (N\geq5)} = 9.7 \times 10^{-4}$ to 1.4×10^{-3}, whereas ≥30 people is $\Sigma P_{SOC\ (N\geq30)} = 1.8$ to 2.6×10^{-4}. Societal risks are lower than those from past New Zealand earthquakes, or storm and flood events, that have killed multiple people.

DOC now needs to evaluate the risk in the context of risk tolerability and value judgements and decide whether the levels of risk at Plateau Hut are tolerable or intolerable. Within DOC’s visitor categories, Plateau Hut is classed as a ‘Backcountry Adventure’ site, which is used mostly but not exclusively by Remote Seeker risk taker visitors (climbers), who have a high risk tolerance because of the activity they are engaging in. On the basis of criteria outlined in 2021 to GNS Science (D Bogie, pers. comm.), the risk is likely to fall in the category ‘substantial yet tolerable’ for those seeking a higher risk experience if risk is reduced to ALARP (as low as reasonably practicable) but may fall in the category of ‘intolerable’ for a user with a low risk profile. Any mountain guides or DOC staff who visit the hut regularly should also consider their annual individual fatality risk (AIFR), being the daily P_{IRPD} risk multiplied by the number of days per year spent at the hut. Risk mitigation may alternatively be required, given that the ‘societal risk’ f/N relationship sits close to tolerable/ALARP thresholds applied elsewhere internationally for societal risk (Strouth and McDougall 2021).

6.0 ACKNOWLEDGEMENTS

The author would like to thank Don Bogie and others at the Department of Conservation for discussion about hazards at Aoraki / Mount Cook and provision of supporting information on visitor use. New data from the Matariki Project, led by Pascal Sirguey (National School of Surveying, University of Otago), has been critical to updating the analysis of risk. Calculations were prepared under the guidance and assistance of Chris Massey and Saskia de Vilder. The report has been reviewed by Andrea Wolter and Saskia de Vilder.

7.0 REFERENCES

[AGS] Australian Geomechanics Society. 2007. Practice note guidelines for landslide risk management. *Australian Geomechanics*. 42(1):63–114.

Allen SK. 2009. Geomorphic hazards associated with glacial change, Aoraki/Mount Cook region, Southern Alps, New Zealand [PhD thesis]. Christchurch (NZ): University of Canterbury. 1 vol.

Allen SK, Cox SC, Owens IF. 2011. Rock avalanches and other landslides in the central Southern Alps of New Zealand: a regional study considering possible climate change impacts. *Landslides*. 8(1):33–48. doi:10.1007/s10346-010-0222-z.

Allen SK, Gruber S, Owens IF. 2009. Exploring steep bedrock permafrost and its relationship with recent slope failures in the Southern Alps of New Zealand. *Permafrost and Periglacial Processes*. 20(4):345–356. doi:10.1002/ppp.658.

Bartelt P, Buser O, Vera Valero C, Bühler Y. 2016. Configurational energy and the formation of mixed flowing/powder snow and ice avalanches. *Annals of Glaciology*. 57(71):179–188. doi:10.3189/2016AoG71A464.

Bartelt P, Christen M, Bühler Y, Buser O. 2018. Thermomechanical modelling of rock avalanches with debris, ice and snow entrainment. In: Cardoso AS, Borges JL, Costa PA, Gomes AT, Marques JC, Vieira CS, editors. *Numerical methods in geotechnical engineering IX*. Boca Raton (FL): Taylor & Francis. p. 1047–1054.

Bradley BA, Bae SE, Polak V, Lee RL, Thomson EM, Tarbali K. 2017. Ground motion simulations of great earthquakes on the Alpine Fault: effect of hypocentre location and comparison with empirical modelling. *New Zealand Journal of Geology and Geophysics*. 60(3):188–198. doi:10.1080/00288306.2017.1297313.

Cox SC, Allen SK. 2009. Vampire rock avalanches of January 2008 and 2003, Southern Alps, New Zealand. *Landslides*. 6(2):161–166. doi:10.1007/s10346-009-0149-4.

Cox SC, Barrell DJA, compilers. 2007. Geology of the Aoraki area [map]. Lower Hutt (NZ): GNS Science. 1 folded map + 71 p., scale 1:250,000. (GNS Science 1:250,000 geological map; 15).

Cox SC, McSaveney MJ, Spencer J, Allen SK, Ashraf S, Hancox GT, Sirguey P, Salichon J, Ferris BG. 2015a. Rock avalanche on 14 July 2014 from Hillary Ridge, Aoraki/Mount Cook, New Zealand. *Landslides*. 12(2):395–402. doi:10.1007/s10346-015-0556-7.

Cox SC, Menzies CD, Sutherland R, Denys PH, Chamberlain C, Teagle DAH. 2015b. Changes in hot spring temperature and hydrogeology of the Alpine Fault hanging wall, New Zealand, induced by distal South Island earthquakes. *Geofluids*. 15(1–2):216–239. doi:10.1111/gfl.12093.

Cox SC, Stirling MW, Herman F, Gerstenberger M, Ristau J. 2012. Potentially active faults in the rapidly eroding landscape adjacent to the Alpine Fault, central Southern Alps, New Zealand. *Tectonics*. 31(2). doi:10.1029/2011TC003038.

de Vilder SJ, Massey CI. 2020a. Guidelines for natural hazard risk analysis on public conservation lands and waters – Part 3: analysing landslide risk to point and linear sites. Lower Hutt (NZ): GNS Science. 52 p. Consultancy Report 2020/52. Prepared for Department of Conservation.

de Vilder SJ, Massey CI. 2020b. Guidelines for natural hazard risk analysis on public conservation lands and waters – Part 4: a commentary on analysing landslide risk to point and linear sites. Lower Hutt (NZ): GNS Science. 64 p. Consultancy Report 2020/53. Prepared for the Department of Conservation.

Fell R, Corominas J, Bonnard C, Cascini L, Leroi E, Savage WZ. 2008. Guidelines for landslide susceptibility, hazard and risk zoning for land use planning. *Engineering Geology*. 102(3–4):85–98. doi:10.1016/j.enggeo.2008.03.022.

Hancox GT, Chinn TJ, McSaveney MJ. 1991. Mt Cook rock avalanche, 14 December 1991. Wellington (NZ): DSIR Geology and Geophysics. 15 p. Immediate Report H36/942.

Hancox GT, Perrin ND, Dellow GD. 2002. Recent studies of historical earthquake-induced landsliding, ground damage, and MM intensity in New Zealand. *Bulletin of the New Zealand Society for Earthquake Engineering*. 35(2):59–95. doi:10.5459/bnzsee.35.2.59-95.

Hancox GT, Ries WF, Lukovic B, Parker RN. 2014. Landslides and ground damage caused by the Mw 7.1 Inangahua earthquake of May 1968 in northwest South Island, New Zealand. Lower Hutt (NZ): GNS Science. 89 p. + 1 folded map. (GNS Science report; 2014/06).

Hancox GT, Ries WF, Parker RN, Rosser BJ. 2016. Landslides caused by the MS 7.8 Murchison earthquake of 17 June 1929 in northwest South Island, New Zealand. Lower Hutt (NZ): GNS Science. 131 p. + 4 maps. (GNS Science report; 2015/42).

Hancox GT, Thomson R. 2013a. Reassessment of geological hazards and risk at Plateau Hut following the rock avalanche from Mt Haast on 21 January 2013 in Aoraki/Mt Cook National Park. Lower Hutt (NZ): GNS Science. 45 p. Consultancy Report 2013/58. Prepared for Department of Conservation.

Hancox GT, Thomson R. 2013b. The January 2013 Mt Haast rock avalanche and Ball Ridge rock fall in Aoraki/Mt Cook National Park, New Zealand. Lower Hutt (NZ): GNS Science. 26 p. (GNS Science report; 2013/33).

Heim A. 1932. Landslides & human lives. Skermer N, translator. Vancouver (CA): BiTech Publishers. 195 p.

Horspool NA, Chadwick MP, Ristau J, Salichon J, Gerstenberger MC. 2015. ShakeMapNZ: informing post-event decision making. In. *New dimensions in earthquake resilience: 2015 New Zealand Society for Earthquake Engineering Technical Conference and AGM*. 2015 Apr 10–12; Rotorua, New Zealand. Wellington (NZ): New Zealand Society for Earthquake Engineering. Paper O-40.

Howarth JD, Barth NC, Fitzsimons SJ, Richards-Dinger K, Clark KJ, Biasi GP, Cochran UA, Langridge RM, Berryman KR, Sutherland R. 2021. Spatiotemporal clustering of great earthquakes on a transform fault controlled by geometry. *Nature Geoscience*. 14(5):314–320. doi:10.1038/s41561-021-00721-4.

Kargel JS, Leonard GJ, Shugar DH, Haritashya UK, Bevington A, Fielding EJ, Fujita K, Geertsema M, Miles ES, Steiner J, et al. 2016. Geomorphic and geologic controls of geohazards induced by Nepal's 2015 Gorkha earthquake. *Science*. 351(6269):aac8353. doi:10.1126/science.aac8353.

LINZ Data Service. 2012. NZ 8m Digital Elevation Model (2012). Wellington (NZ): Land Information New Zealand; [updated 2016 Aug 18; accessed 2021 Aug 27]. https://data.linz.govt.nz/layer/51768-nz-8m-digital-elevation-model-2012/

Malamud BD, Turcotte DL, Guzzetti F, Reichenbach P. 2004. Landslide inventories and their statistical properties. *Earth Surface Processes and Landforms*. 29(6):687–711. doi:10.1002/esp.1064.

Massey CI, de Vilder SJ, Taig T, Lukovic B, Archibald GC, Morgenstern R. 2019. Landslide hazard and risk assessment for the Fox and Franz Josef Glacier valleys. Lower Hutt (NZ): GNS Science. 79 p. + appendices. Consultancy Report 2018/206. Prepared for Department of Conservation.

Massey CI, Lukovic B, Huso R, Buxton R, Potter SH. 2021. Earthquake-induced landslide forecast tool for New Zealand: version 2.0. Lower Hutt (NZ): GNS Science. 77 p. (GNS Science report; 2018/08).

Massey CI, Townsend DT, Lukovic B, Morgenstern R, Jones K, Rosser B, de Vilder S. 2020. Landslides triggered by the M_W7.8 14 November 2016 Kaikōura earthquake: an update. *Landslides*. 17(10):2401–2408. doi:10.1007/s10346-020-01439-x.

Massey CI, Townsend DB, Rathje E, Allstadt KE, Lukovic B, Kaneko Y, Bradley B, Wartman J, Jibson RW, Petley DM, et al. 2018. Landslides triggered by the 14 November 2016 Mw 7.8 Kaikoura earthquake, New Zealand. *Bulletin of the Seismological Society of America*. 108(3B):1630–1648. doi:10.1785/0120170305.

McDougall S. 2017. 2014 Canadian Geotechnical Colloquium: landslide runout analysis – current practice and challenges. *Canadian Geotechnical Journal*. 54(5):605–620. doi:10.1139/cgj-2016-0104.

McSaveney MJ. 2002. Recent rockfalls and rock avalanches in Mount Cook National Park, New Zealand. In: Evans SG, DeGraff JV, editors. *Catastrophic landslides: effects, occurrence, and mechanisms*. Boulder (CO): Geological Society of America. p. 35–70. (Reviews in engineering geology; 15).

McSaveney MJ, Cox SC, Hancox GT. 2014. Seeking a credible cause of the recent increase in rock-avalanche frequency in New Zealand's Southern Alps [abstract]. In. *AGU Fall Meeting*; 2014 Dec 15–19; San Francisco, CA. Washington (DC): American Geophysical Union. abstract NH41A-3775.

McSaveney MJ, Cox SC, Hancox GT. 2015. Increasing rock-avalanche frequency correlates with increasing seismic moment release in New Zealand's Southern Alps. In: *European Geosciences Union General Assembly 2015*; 2015 Apr 12–17; Vienna, Austria. Goettingen (DE): Copernicus Gesellschaft. Abstract EGU2015-8074.

Orchiston C, Mitchell J, Wilson T, Langridge R, Davies T, Bradley B, Johnston D, Davies A, Becker J, McKay A. 2018. Project AF8: developing a coordinated, multi-agency response plan for a future great Alpine Fault earthquake. *New Zealand Journal of Geology and Geophysics*. 61(3):389–402. doi:10.1080/00288306.2018.1455716.

Sattler K, Anderson B, Mackintosh A, Norton K, de Róiste M. 2016. Estimating permafrost distribution in the maritime Southern Alps, New Zealand, based on climatic conditions at rock glacier sites. *Frontiers in Earth Science*. 4:4. doi:10.3389/feart.2016.00004.

Stark CP, Hovius N. 2001. The characterization of landslide size distributions. *Geophysical Research Letters*. 28(6):1091–1094. doi:10.1029/2000GL008527.

Stirling MW, McVerry GH, Gerstenberger MC, Litchfield NJ, Van Dissen RJ, Berryman KR, Barnes P, Wallace LM, Villamor P, Langridge RM, et al. 2012. National seismic hazard model for New Zealand: 2010 update. *Bulletin of the Seismological Society of America*. 102(4):1514–1542. doi:10.1785/0120110170.

Strouth A, McDougall S. 2021. Societal risk evaluation for landslides: historical synthesis and proposed tools. *Landslides*. 18(3):1071–1085. doi:10.1007/s10346-020-01547-8.

Taig T, McSaveney MJ. 2015. Milford Sound risk from landslide-generated tsunami. Lower Hutt (NZ): GNS Science. 57 p. Consultancy Report 2014/224. Prepared for Environment Southland.

Van Houtte C, Gerstenberger MC. 2019. Potential short-term aftershock sequences of an Alpine Fault earthquake and their ground motion fields. Lower Hutt (NZ): GNS Science. 23 p. (GNS Science report; 2019/13).

www.gns.cri.nz

Principal Location

1 Fairway Drive, Avalon
Lower Hutt 5010
PO Box 30368
Lower Hutt 5040
New Zealand
T +64-4-570 1444
F +64-4-570 4600

Other Locations

Dunedin Research Centre
764 Cumberland Street
Private Bag 1930
Dunedin 9054
New Zealand
T +64-3-477 4050
F +64-3-477 5232

Wairakei Research Centre
114 Karetoto Road
Private Bag 2000
Taupo 3352
New Zealand
T +64-7-374 8211
F +64-7-374 8199

National Isotope Centre
30 Gracefield Road
PO Box 30368
Lower Hutt 5040
New Zealand
T +64-4-570 1444
F +64-4-570 4657